AAAM 64th Annual Scientific Conference

October 12 - October 16, 2020

Student Symposium Presentations

Target Population for Motorcycle-Detecting Automatic Emergency Braking Systems

Morgan E. Dean
Samantha H. Haus, Hampton C. Gabler
Virginia Tech

INTRODUCTION

In 2017 in the U.S., there were 5,172 motorcyclist fatalities and approximately 89,000 motorcyclists injured [1]. Active safety systems, such as automatic emergency braking (AEB), have the potential to reduce these numbers by mitigating and preventing crash and injury severity. AEB is an effective countermeasure in detecting and avoiding both rear crashes and collisions with pedestrians. However, the potential effectiveness of motorcycle-detecting AEB (MD-AEB) is currently unknown.

The goal of this study was to determine the target population which could be prevented or mitigated by MD-AEB and characterize any environmental or crash factors which could reduce MD-AEB effectiveness.

METHODS

Data Sources

This study's data came from both NHTSA's Fatality Analysis Reporting System (FARS) and General Estimates System (GES). FARS is a census of all fatal crashes that occurred on public roads in the United States [2]. GES is a probability sample of police-reported crashes in the U.S. (including fatal cases). Collected from 60 locations across the U.S., GES cases are assigned sampling weights which, when applied to each case, can estimate the national incidence of various crash types [3]. This study used case years 2011-2015.

AEB Design Constraints

Certain crash conditions may reduce the performance of active safety systems. AEB system design therefore requires careful consideration of the following constraints.

1. Crash configuration: AEB systems rely on forward-facing sensors and so are expected to be most effective in front-to-rear crashes. Therefore, initial AEB systems will be most effective in cases where the rider is traveling in the same lane or an adjacent lane to an AEB-equipped car. AEB may be less effective in intersection/crossing path configurations, as there would be less time for detection and for the system to react. AEB would not be an effective countermeasure in single vehicle crashes, and sideswipe crashes would be better handled by blind spot monitoring.
2. Pre-event vehicle movement: AEB may have reduced effectiveness in turning scenarios as a narrow sensor field of view may not detect all potential collision partners.
3. Evasive maneuvers: some AEB systems deactivate when the driver brakes or steers.
4. Obstructions: obstructions may prevent sensors from seeing a motorcycle. The assumption will be that obstructions reported by the driver would also hinder detection by the sensors.
5. Vehicle speed: an increased vehicle speed would decrease the system's time to react.
6. Environmental conditions: some sensors, e.g. cameras, may be less effective in low light while other sensors, e.g. radar, may be less effective in rain or snow.

RESULTS

Determining the Target Population

This study began by examining two-vehicle crashes where at least one of the vehicles was a motorcycle. Single motorcycle crashes were excluded because a vehicle-mounted AEB system would not be an applicable countermeasure. Multiple vehicle crashes (3+ vehicles) were excluded due to the difficulty of determining vehicle roles and configurations within the crash. As shown in Figure 1, two-vehicle motorcycle crashes make up half of all annual police-reported and fatal motorcycle crashes.

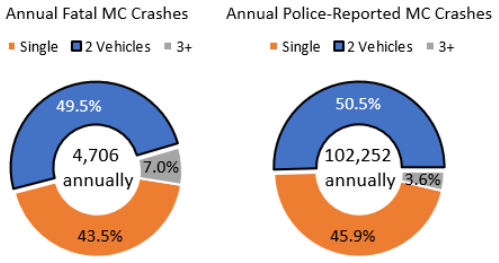

Figure 1. Number of vehicles involved in all police-reported (GES) and fatal (FARS) motorcycle crashes.

Only passenger vehicles (PVs), which include cars and light trucks and vans (LTVs), are likely to be equipped with initial MD-AEB systems. Therefore, only two-vehicle crashes which included one motorcycle and one PV were included in the target population. Under the assumption that a motorcycle was vehicle one, two-vehicle motorcycle crashes were then grouped by the vehicle type of vehicle two. For fatal crashes, a PV was the most common (86%) second vehicle (upper left in Figure 2).

Additionally, AEB systems use a combination of forward-facing radar and forward-facing cameras to detect motorcyclists, so only cases where a passenger vehicle struck a motorcycle with its front end were considered relevant crash scenarios. Within the motorcycle-PV crash population, the motorcycle was the striking vehicle 63% of the time. In a surprisingly small percentage of cases (19%), the motorcycle was struck by the PV (upper right in Figure 2). The 'acctype' variable was used to determine striking and struck roles, a method which has room for future improvements. The 19% of crashes where motorcycles were struck was then broken down by the PV's area of impact. For 93% of the crashes, the PV had a frontal impact (bottom chart in Figure 2). This selection process and its associated assumptions yielded an annual fatal target population of 358 crashes.

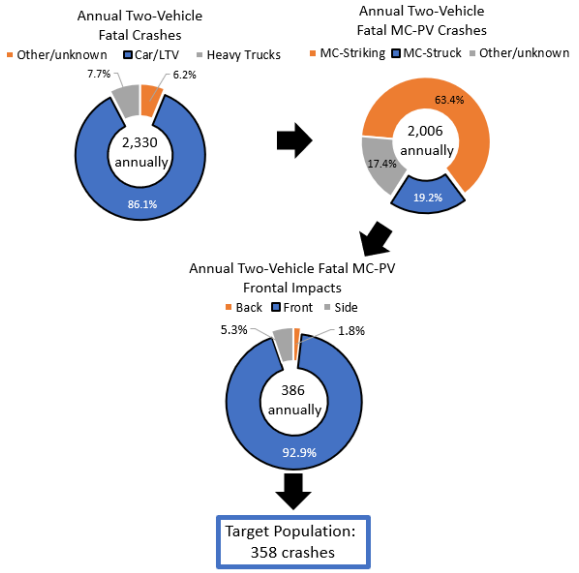

Figure 2. Target population inclusion criteria for fatal crashes (FARS). Inclusion criteria include the second vehicle type (upper left), the role of the MC (upper right), and the PV impacted area (bottom).

For police-reported, two-vehicle motorcycle crashes, the motorcycle collided with a PV 95% of the time (upper left in Figure 3). Within that 95%, the motorcycle was most often (63%) the striking vehicle, much like with the fatal crash population. For 23% of the crashes, the PV struck the motorcycle, which indicates potential for MD-AEB application (upper right in Figure 3). Of the PV-striking-motorcycle cases, 86% of the PVs suffered a frontal impact (bottom chart in Figure 3). This yielded a police-reported target population of 9,659 crashes annually.

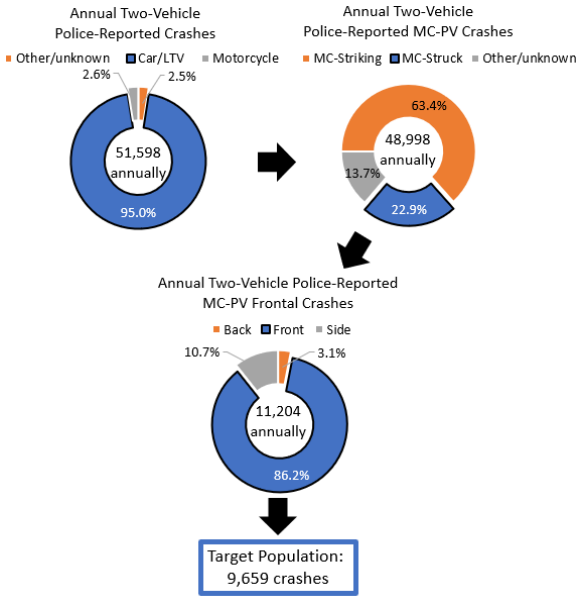

Figure 3. Target population inclusion criteria for police-reported crashes (GES). Inclusion criteria include the second vehicle type (upper left), the role of the MC (upper right), and the PV impacted area (bottom).

This target population accounts for 8% and 10% of all fatal and police-reported motorcycle crashes, respectively. It excludes sideswipe crashes and cases where the passenger vehicle lost control, as AEB could not prevent a crash, for example, if the vehicle lost traction. An AEB system would most likely not be 100% effective, so this target population is an upper bound.

Characterizing the Target Population

The second half of this study characterized the MD-AEB target population by crash and environmental factors. Crash factors examined in this study were crash configuration, posted speed limit, PV driver vision obstruction, PV pre-vehicle movement, and PV evasive maneuver. Environmental factors were lighting and weather conditions.

Crash Characteristics. The motorcycle suffered a frontal collision in the majority of fatal crashes (37%) and was struck in the rear in the majority of police-reported crashes (54%). The most common posted speed limit for fatal crashes was 55 mph (29%), as opposed to 35 mph for police-reported crashes (22%). Most often, the PV's driver's vision was not obscured (95% fatal, 92% police-reported). In 50% of fatal

crashes, the PV had been travelling straight prior to the collision, compared to 62% for police-reported crashes. The PV was negotiating a curve prior to the collision in 24% of fatal crashes. This was 13 percentage points above the second most common movement in police-reported crashes (starting in road, 11%). In 63% of fatal crashes no avoidance maneuver was made by the driver of the PV. For 28% of fatal crashes it was unknown whether an avoidance maneuver was attempted. For police-reported crashes, the avoidance maneuver was most often unknown (54%) with no avoidance maneuver as the second most common category (30%).

Environmental Characteristics. Most fatal and police-reported collisions occurred in daylight (60% and 65%, respectively). Darkness (both lighted and unlighted) was the second most common condition for both datasets. Clear weather conditions existed for 83% (fatal) and 87% (police-reported) of crashes. Cloudy conditions comprised approximately 12% of crashes in both datasets, with rain occurring 3% for both.

DISCUSSION

The target population for MD-AEB represents an upper bound on the potential effectiveness of this active safety system. However, several factors may reduce the potential effectiveness of MD-AEB. AEB may have limited effectiveness in adverse weather and low light conditions. Wet roads could alter the effectiveness of braking. Additionally, some AEB systems rely on both radar and camera object-recognition before they take action [4]. While adverse conditions may not severely inhibit radar performance, poor weather or lighting could have an adverse effect on camera performance. Most target population crashes occurred in clear weather conditions and daylight, but about 30% of fatal crashes occurred in dark lighting conditions. AEB may also have reduced effectiveness in turning scenarios since the driver's field of view is reduced and surrounding vehicles may move in and out of view. While the majority of passenger vehicles were travelling straight prior to fatal crashes, a quarter of them were negotiating a curve.

This analysis was limited by the information available in the datasets. For example, GES cases are weighted to estimate national incidence for each case. Additionally, FARS and GES do not include scene diagrams so specific collision configurations could not be simulated. The role of the motorcycle could not be determined for about 15% of the two-vehicle MC-PV crashes. An improved methodology for determining vehicle roles may reveal a slightly larger target population than determined here. For now, this target population remains a conservative upper bound.

CONCLUSION

The target population for MD-AEB represents an upper bound on the potential effectiveness of this active safety system. The system was assumed to be applicable to two-vehicle crashes wherein a PV was frontally impacted upon striking a motorcycle. This target population comprised only a small fraction of the total motorcycle crash population (only 8% of fatal and 10% of police-reported motorcycle crashes). Half of all motorcycle crashes are single vehicle collisions for which AEB would not be applicable. In two-vehicle collisions, MD-AEB would be most applicable in collisions in which the motorcycle was the struck vehicle. However, it is more common for motorcycles to be the striking rather than the struck vehicle.

NOVELTY/TRAFFIC SAFEY IMPLICATIONS

These characteristic distributions will aid in the development of potential safety benefit models by indicating factors that increase risk of collisions and estimating the number of crashes that may not be able to be avoided by a motorcycle-detecting AEB system.

ACKNOWLEDGEMENTS

The authors would like to acknowledge the Toyota Collaborative Safety Research Center (CSRC) and Toyota Motor Corporation for funding this research study.

REFERENCES

[1] National Highway Traffic Safety Administration, "Traffic Safety Facts 2017: A Compilation of Motor Vehicle Crash Data," DOT HS 812 806, 2019.

[2] National Highway Traffic Safety Administration, "Fatality Analysis Reporting System (FARS): Analytical User's Manual, 1975-2017." 2018.

[3] National Highway Traffic Safety Administration, "National Automotive Sampling System (NASS) General Estimates System (GES): Analytical User's Manual, 1988-2015." 2019.

[4] R. Ono, W. Ike, and Y. Fukaya, "Pre-Collision System for Toyota Safety Sense," in *SAE 2016 World Congress and Exhibition*, Apr. 2016, doi: https://doi.org/10.4271/2016-01-1458.

Active safety systems for motorcycles: where are we? A novel transnational comparison of applicability in the Australian, American and Italian fleets

Paolo Terranova[a], Morgan Dean[b], Hampton C. Gabler [ab], Simone Piantini[a], Giovanni Savino[ac]

[a] Dept. of Industrial Engineering – DIEF, University of Florence, Florence, Italy.
[b] Dept of Biomedical Engineering and Mechanics, Virginia Tech, Blacksburg, Virginia, USA.
[c] Monash University Accident Research Centre, Melbourne, Australia.

INTRODUCTION

Motorcycle-based active safety systems have great promise to avoid or mitigate many of the crashes suffered by motorized two-wheeled motorcyclists (PTW). PTW crashes account for a large proportion of traffic fatalities globally, with motorcyclists representing 25,3%, 13,7% and 15,4% of road deaths in Italy, Australia and USA respectively. Active safety systems, such as automated emergency braking and electronic stability control, have proven to be very effective in the 4-wheeled vehicle fleet. But in the motorcycle fleet, most systems are still only in the prototype stage. In order to direct the research it is necessary to understand which active safety systems have the greatest chance of reducing crashes. Our hypothesis is that regional differences in PTW accident type, motorcycle type and road systems could lead to different region-specific priorities for developing safety systems.

Research question / Objective

The aim of the study is to compare the applicability of PTW active safety systems in the US, Australia and Italy, using police-reported accident data in each region. The goal is to understand which active systems could have the greatest likelihood of reducing PTW crashes in each country.

METHODS

Country-specific applicability was estimated based on the approach used in an earlier Australian study [2] with a few modifications made to accommodate Italian and US crash data. The five most promising PTW active safety systems [1] were considered: anti-lock braking (ABS), motorcycle automated emergency braking (MAEB), collision warning, curve warning and curve assist. In the original study [2], an expert panel assessed the expected applicability of each PTW technology to avoid or mitigate each crash type. Crash type was categorized using the VicRoads Definition for Classifying Accidents (DCA) crash type scheme [3]. Applicability scores ranged from 4 (definitely applicable) to 1 (not applicable). In our study, these applicability scores were assigned to each crash type in Italy and US and compared to detect region-specific differences.

Data sources

The Italian dataset was comprised of 294 cases from the newly developed Prato-X database that contains PTW crashes which occurred in the Municipality of Prato in 2018. The US dataset was comprised of 5894 cases from the US Crash Reporting Sampling System (CRSS) from the years 2016-2018. CRSS sampling weights were applied in all CRSS calculations, resulting in an estimated total of 265361 US crashes. These data were compared with data from crashes that occurred in Victoria, Australia from 2000-2011 [2]. In the CRSS database, only crashes that occurred on urban roads were considered, in order to better compare with the crashes in the Municipality of Prato.

One major difference between the three regions is the large number of PTWs present in Italy [4] compared to the US and Australia. This is despite the fact that the ratio between people and registered vehicles is almost the same for the three countries (I = 1,17; US = 1,20; Victoria = 1,33). In Italy in 2018 there were 51.682.370 registered vehicles, of which 6.780.733 were PTW (13,1%). This percentage remains similar considering Tuscany (region that contains the Municipality of Prato) and Prato: 15,8% and 11,7% respectively. Instead in the Victoria region in 2011 there were 161.261 PTW (3,9% of the total vehicles). In the USA in 2018 there were 8.666.185

PTW, i.e. 3,2% of the total of registered vehicle. For the Municipality of Prato, 2018 represented a particular year as there were no people who died in accidents involving PTW.

Accident classification

The study first recoded the accident types of U.S. and Italian data using the DCA code after first adjusting the codes for driving on the right side of the road. The DCA chart is divided into 10 categories and altogether there are 81 types of accident scenarios each described by a pictogram containing the trajectory of the vehicles involved in the crashes. As done in [2] it was necessary to extend the accident configuration from 82 to 152 as the DCA code does not specify the type of vehicle to which the number corresponds. The expansion was therefore made to be able to consider all possible combinations of the position of motorcycles, machines and other vehicles. In the classification of Prato, unlike the Australian study, a second variable was introduced for the scenarios of loss of control (from 170 to 184) and of maneuvers (from 140 to 148). This variable is intended to better specify the "Scenario/Cause" in the case of loss of control and the "Manner of Impact" in the case of maneuvers. In fact, for some crashes, (e.g. loss of control caused by emergency braking aimed at avoiding other crashes, or maneuvers where the type of impact is very different from that shown in the pictogram) the DCA classification in an event was considered insufficient and the number of variables was increased to better classify the accident. To study the applicability in the US fleet, AccType, the crash type classification scheme, used in CRSS [5] was first translated to DCA codes (right drive). Additional CRSS variables were used as needed to identify the corresponding DCA scenarios. But despite this it was not possible to translate all the scenarios.

Determination of the relevance of the safety system selected for motorcycle crashes

After coding the crashes in Prato-X and CRSS, the applicability of the five safety systems in the various scenarios was evaluated using the method in the original Australian study [2]. For AccType scenarios that could not be translated into the DCA code, an applicability assessment was made based on the definition of the categories used for the Australian DCA assessment (tab. 1 [2]).

RESULTS

The main purpose of this article was to evaluate the percentage of major crashes in each category for each of the safety systems, and to make a comparison between the three countries. As can be seen in Table 1, ABS is relevant (categories 2, 3 and 4) in 91,2% of crashes in Prato, 92,2% in Victoria and 84,6% in the US. For the MAEB, on the other hand, it is definitely applicable (category 4) in 10,5% of Prato crashes, in 5,7% in Victoria and in 11,6% in the US. As for the collision warning, it was considered relevant (2,3 and 4) in the 80,4% of crashes in Prato, in the 57,7% in Victoria and in the 67.3% in the US. The Curve Warning is considered irrelevant (category 1) in the 90,9% of Prato crashes, in the 79,1% in Victoria and in the 58,2% in the US. Curve Assist is not relevant in the 70,2% of Prato crashes, in the 43,5% in Victoria and in the 72% in the US. The safety system with the highest percentage of crashes classified in category 4 was ABS (P = 74,7%, Vict = 40,6%, USA = 27,2%), followed by the collision warning (P = 40%, Vict = 23,1%, USA = 21,2%). The category 2 and 3 of relevance is particularly important for MAEB is worth 68,1% of crashes in Prato, in 41,6% in Victoria and in 55,6% in the US.

DISCUSSION

One of the challenges of this study has been that accident types are coded quite differently from country to country. This was especially true in multi-event crashes. The Australian categorization used the DCA [3] but only considered the first crash event. In Prato the DCA was used but considered both the 1st and 2nd events. In the US, CRSS uses the Acctype classification which could not always be readily translated to DCA. Specifically, a large number of CRSS cases had an Acctype "Other" or "Unknown". These cases could not be accurately translated into DCA. For example, category 4 of ABS, shows very different values among the 3 countries examined. Applicability was much lower for ABS in the US (27,2%) than Italy or Australia. Both the 'Other' and 'Unknown' scenarios were assigned an ABS rating of 2 (category 2 means "possible / perhaps applicable"). The large number of US crashes contained in these two scenarios unbalanced the results by making category 2 weigh much more than the others.

On the other hand, reliable results were obtained for category 3 of the MAEB. The large difference between Prato and US/Victoria is due to the greater number of side banks (they have a rating of 3 at the MAEB): in Prato they represent 23,86% of the total crashes, while in the US they are 10,33%. This different percentage reflects the different traffic conditions between the two countries. In Italy, it is normal for PTWs to pass between lines of stopped vehicles but is the main cause of crashes with lateral rubbing The definition of category 3 (probably

Safety Sistem	Category 1 (not relevant)			Category 2 (possible)			Category 3 (probably)			Category 4 (definitely)		
	Prato	USA	Victoria	Prato	USA	Victoria	Prato	USA	Victoria	Prato	USA	Victoria
ABS	8,8%	15,4%	7,1%	13,0%	54,3%	49,3%	3,5%	3,1%	2,3%	74,7%	27,2%	40,6%
MAEB	21,4%	32,8%	52,1%	27,0%	47,5%	24,3%	41,1%	8,1%	17,3%	10,5%	11,6%	5,7%
Collision warning	19,6%	32,7%	41,6%	3,9%	37,4%	14,1%	36,5%	8,7%	20,5%	40,0%	21,2%	23,1%
Curve warning	90,9%	58,2%	79,1%	4,6%	32,2%	4,4%	0%	0%	0%	4,6%	9,6%	15,8%
Curve assist	70,2%	72,0%	43,5%	22,8%	14,7%	36,6%	2,5%	3,4%	3,2%	4,6%	9,9%	16,1%

Table 1. Applicability of PTW Active Safety Systems in the 3 countries

applicable) [2] says "It probably would have applied - the technical challenges have yet to be resolved". Collision Warning Category 3 and MAEB are very relevant. Systems like MAEB and Collision Warning require obstacle detection systems, so this is an area where future development could be useful. In fact, from the results we see how a development of the MAEB aimed to allow activation in the event that the opposite vehicle is front/side (for example, sideswipe) would have a great applicability, increasing the percentages of category 4 by removing the scenarios from the category 3.

Based on category 4 of the MAEB, this system has much greater applicability in the US and Prato than in Victoria. This may be because the Victoria system only classifies crashes by first event, which may lead to an underestimation of MAEB applicability. In fact, the classification of a second event was very important in the categorization of crashes in Prato. For example, there were 28 rear-end collisions with PTW behind the vehicle (category 4 for MAEB), 9,8% of the total. 10 of these 28 have been classified as 1st event 174 and 2nd rear-end event, as the first event is the loss of control of the vehicle caused by emergency braking to try to avoid the rear collision. Without using a 2nd event, these 10 incidents would have been classified as loss of control and consequently the applicability of the MAEB would have been underestimated.

Table 1 shows that Curve Warning and Curve Assist had poor applicability in Prato (Warning = 4,6%; Assist = 4,6%) where only urban crashes were examined. Even in the US only urban crashes were examined, however the percentage was almost double (Warning = 9,6%; Assist = 9,9%). This demonstrates the possible utility that these systems would have in the US. For Australia the percentage was much higher (Warning = 15,8%; Assist = 16,1%) because crashes in the whole Victoria region were considered, including motorways and roads outside the city.

NOVELTY/TRAFFIC SAFETY IMPLICATIONS

This study has shown that the applicability of production or anticipated PTW active safety systems, e.g., MAEB, is likely to be a strong function of the country into which these countermeasures are introduced. This has important implications for manufacturers seeking to prioritize the development of active safety countermeasures for a particular PTW fleet. In addition, because active safety countermeasures may differ by motorcycle type, these regional differences suggest that regulators may need to consider country-specific minimum performance standards.

REFERENCES

[1] Gil G, Savino G, Piantini S, Baldanzini N, Happee R, Pierini M. Are automatic systems the future of motorcycle safety? A novel methodology to prioritize potential safety solutions based on their projected effectiveness. Traffic Inj Prev. 2017a; 18:877–885.

[2] Giovanni Savino, Marco Pierini & Michael Fitzharris (2019): Motorcycle active safety systems: Assessment of the function and applicability using a population-based crash data set, Traffic Injury Prevention, vol. 20, issue 4, 2019

[3] Crashstats User Guide, Road Crash Statistics, Victoria, 2013 Edition, Appendix C, p. 44-45

[4] ISTAT (National Institute of Statistics), Road Accident, Annual Report 2018, 2019. Data compared with another source: Decentralized Collection in the Tuscany Region (SIRSS PROJECT)

[5] National Center for Analysis and Statistics. (2019, November). *Crash Report Sampling System CRSS analytical user's manual 2016-2018* (Report No. DOT HS 812 846). National Highway Traffic Safety Administration - U.S.A.

Construction of Injury Prediction Model Using Random Forest Algorithm with Resampling Methods for Imbalanced Accident Data

Kotaro Otsuka †
† Tokyo Institute of Technology

Kei Sakamoto †, Yusuke Miyazaki †, Fusako Sato ‡, Kouji Kitamura *
‡ Japan Automobile Research Institute, * National Institute of Advanced Industrial Science and Technology

INTRODUCTION

Traffic accident data analyses are fundamental for the development of countermeasures to mitigate fatalities and injuries. Analysis results have been used to evaluate risk factors in real-world accidents, effectiveness of interventions, and development of advanced protective devices. In the analyses, injury risk probability was modeled using statistical predictive methods. For example, logistic regression methods have mostly been applied to develop a statistical function to predict injury risk from contributing factors [1]. Although logistic regression models assume a linear relationship between risk factors and contributing factors, the relationship may be nonlinear. Therefore, machine learning methods that can deal with nonlinear relationships could more accurately estimate the injury risks. In addition, the field accident data are essentially imbalanced data. In other words, the number of minor injuries is much higher than that of severe injuries or deaths. Accordingly, the application of a data resampling algorithm to the imbalanced data may also contribute to improving the accuracy of the injury prediction model.

Therefore, this study aimed to construct an injury prediction model using a nonlinear machine learning model, the random forest (RF), based on collision conditions, occupants, and vehicle factors, by applying resampling algorithms for an imbalanced dataset and also compared the prediction accuracy with the logistic regression model.

METHODS

Data and Inclusion Criteria

The National Automotive Sampling System-Crashworthiness Data System (NASS-CDS) data provided by National Highway Traffic Safety Administration (NHTSA) for the years from 2001 to 2015 were selected as the dataset. The basic inclusion criteria were that sedans, sports utility vehicles (SUVs), vans, and pickup trucks were included. Then, collisions between only two vehicles were included. Occupants who were over 15 years old were included. Finally, only the data for the occupants with the highest score of the Maximum Abbreviated Injury Scale (MAIS) in each vehicle were included. The data inclusion criteria were mostly the same as those in Ref. [2]. The final number of data included was 21,650.

Contributing factors to be included and their grouping

MAIS3+ was set as the predicted variable. The types of explanatory variables that contributed to MAIS3+ were divided into three main categories: collision conditions, vehicles, and occupant factors. For collision conditions, collision position of the own vehicle, collision position of the other vehicle, Delta-V, direction of collision (PDOF), and the features of behavior before collision (collision scenario) were used. The vehicle attributes were vehicle types and weights of both vehicles, weight ratio of the own vehicle to the other vehicle, and features of the model year. Airbags, seat belts, seat position, age, sex, and body mass index (BMI) were selected as occupant factors. These explanatory variables were appropriately categorized to be usable for the RF algorithm. Some features, such as BMI, were created by combining multiple features. These variables are shown in Table 2.

Resampling

Generally, traffic accident data are imbalanced in terms of the ratio between fatalities/severe injuries and minor injuries. However, using such imbalanced data to construct a predictive model results in most of the data being estimated as a majority class. To solve the problem, some resampling algorithms with cost-aware learning and data-level approaches have been proposed. In this study, data-level approaches, which includes oversampling, undersampling, and the hybrid method, were used as resampling algorithms.

Oversampling is a technique used to eliminate bias in the number of data by increasing the number of minority samples. In this study, Random Over Sampling (ROS), Synthetic Minority Oversampling Technique (SMOTE), Adaptive Synthetic (ADASYN), and Borderline-SMOTE (BSMOTE) were examined as oversampling techniques.

Undersampling is a technique to eliminate bias in the number of data by reducing the majority sample. In this study, Random Under Sampling (RUS), Cluster Centroids (CC), and Tomek Links Under Sampling (TLUS) were selected as undersampling methods.

The hybrid method eliminates the bias in the number of data by combining oversampling and undersampling algorithms. In this study, combinations of TLUS, ROS, SMOTE, ADASYN, and BSMOTE were used. After TLUS was applied to the base data, each oversampling algorithm was performed.

Random Forest algorithm

The RF algorithm is a method used to perform ensemble learning whereby the decision tree is regarded as a weak learner. For each decision tree T_i, a bootstrap sample B_i, which is the training data, was created and the number of features that could be used for partitioning was limited by the square root of the total number. The Gini impurity, expressed in the following equation, was used as the basis for the partitioning.

$$I_t = 1 - \sum_c p(c|t)^2 ,$$

where I_t is the Gini impurity at node *t* and $p(c|t)$ is the fraction of class c at node t. The estimation results were obtained by taking the additive average of the probability $p_i(c)$ and a class c, obtained from each of the n decision trees T_i created similarly.

$$p(c) = \frac{1}{n}\sum_i^n p_i(c)$$

Accuracy verification was performed for each resampling algorithm. On the other hand, cost-aware learning was performed for the TLUS data. The weight W_c of class c in cost-aware learning is expressed by the following equation. The number of all data is N, the number of classes is C, and the number of data in class c is N_c.

$$W_c = \frac{N}{C \times N_c}$$

Flow: Model Construction and Accuracy Verification

From the total data 64 % was divided into training data, 16 % into validation data, and the remaining 20 % into test data. Meanwhile, the ratio of all data to MAIS3+ should be equal so that the number of MAIS3+ data is not biased for each segment of data. Next, *K*-fold cross-validation was performed using the training and validation data to determine the hyperparameters. In this study, *K*-fold cross-validation was performed with $K = 5$. Finally, using the searched hyperparameters, we again trained with the combined training and validation data and verified the accuracy with test data.

RESULTS

The grid search for the hyperparameters was performed for three parameters. The numbers of decision trees (n_estimates) were 100, 300, and 500; the depths of the decision trees (max_depth) were 12, 14, 16, 18, and 20; and the numbers of samples of nodes to stop splitting (min_samples_split) were 10, 20, and 30. To deal with imbalanced data, *F*-measure was used as an evaluation index.

The model was constructed and estimated 10 times for the test data with the hyperparameters determined for each resampling method, and the means of *F*-measure and Receiver Operating Characteristic–Area Under the Curve (ROC–AUC) were calculated, respectively.

Table1 shows highest F-measure and its ROC-AUC and hyperparameters of each resampling method. Using the highest *F*-measure in Table 1 (the resampling method: TLUS, the number of decision trees: 100, the depth of the decision trees: 20, and the number of samples of nodes to stop splitting: 10),

Table 1. Test Data Result

Sampling Method	F	ROC-AUC	max_ depth	n_ estimates	min_ samples _split
TLUS	0.533	0.867	20	100	10
No Resampling	0.522	0.872	20	500	20
TLUS + BSMOTE	0.516	0.856	20	500	20
BSMOTE	0.514	0.858	18	100	30
ROS	0.513	0.870	18	500	30
TLUS + ROS	0.510	0.871	16	500	30
TLUS + ADASYN	0.509	0.854	20	300	20
ADASYN	0.508	0.851	18	300	20
SMOTE	0.508	0.855	18	500	30
TLUS + SMOTE	0.507	0.855	18	500	30
RUS	0.468	0.870	20	500	30
CC	0.452	0.866	16	500	20

Table 2. Features and Its Importance

Feature	NASS-CDS Feature	Number of Group	Importance ($\times 10^{-2}$)
Delta-V	DVTOTAL	8	30.5
Collision Scenario	ACCTYPE	14	9.42
The Other Vehicle Collision Position	GADEV1,2	4	8.04
Weight Ratio	CURBWGT, otvehwgt	6	5.97
Seat Belt	MANUSE	2	5.71
BMI	WEIGHT, HEIGHT	6	5.44
PDOF	PODF1	12	5.41
Age	AGE	3	4.09
The Other Vehicle Type	BODYTYPE	4	4.02
Model Year	MODELYR	4	3.92
Vehicle Type	BODYTYPE	4	3.24
Collision Position	GADEV1,2	4	3.15
Seat Position	SEATPOS	2	2.40
Sex	SEX	2	2.04
The Other Airbag	BAGAVAILB AGAVOTH	2	1.64
The Other Vehicle Weight	CURBWGT, otvehwgt	3	1.41
Weight	CURBWGT, otvehwgt	3	1.39
Airbag	BAGAVAIL, BAGAVOTH	2	1.37
Seat Row	SEATPOS	2	0.87

we again used all the data to build the model and calculate the importance of these features.

The mean of the 10 resamples and the model construction are shown on the right side of Table 2. Delta-V was the most important feature, followed by Collision Scenario and The Other Vehicle Collision Position.

DISCUSSION

Upon comparison of resampling algorithms, the *F*-measures of RUS and CC were found to be lower than that of the other methods. However, there was no significant difference for the other methods. The accuracies of the RUS and CC were low because the number of data used for training before resampling was 17,321, while the number after resampling was very small (3846).

In consideration of the importance of these features, it is reasonable for Delta-*V* to have the highest importance because it is considered to be strongly correlated with the increase of kinematic energy transferred by the collision. For Collision Scenario, this may function as a combination of collision condition features, since Collision Scenario implies collision positions, PDOF etc.

To evaluate accuracy of the injury prediction model based on RF, this study also developed logistic regression models using the *F*-measure as an evaluation index when searching for hyperparameters. As the results, the injury prediction model based on RF with TLUS has the highest estimation accuracy as shown in Table 3. Only the best results are shown for both resampling methods.

Table 3 Comparison with other methods

		F	ROC-AUC
Random Forest	TLUS	0.533	0.866
	No Resampling	0.522	0.872
Logistic Regression	ROS	0.485	0.874
	No Resampling	0.482	0.875

CONCLUSION

An RF algorithm, which is a nonlinear machine learning algorithm, was used to construct an injury prediction model with resampling algorithms for imbalanced data. As a result, the proposed method predicted MAIS3+ risk was more accurate than that of the logistic regression algorithm.

NOVELTY/TRAFFIC SAFETY IMPLICATIONS

We improved the accuracy of the injury prediction model using RF. Furthermore, we investigated the effectiveness of resampling algorithms for imbalanced traffic accident data.

REFERENCES

[1] Malliaris A.C, Digges K.H, DeBlois J.H. Relationships between crash casualties and crash attributes, SAE International Congress & Exposition Paper, Detroit, MI, 24-27 February 1997, 970393.
[2] Antona-Makoshi, J., Mikami, K., Lindkvist, M., Davidson, J., Schich, S. Accident analysis to support the development of strategies for the prevention of brain injuries in car crashes. Accident Analysis and Prevention, August 2018, *117*, pp. 98–105.

Development of a Method to Measure Intracranial Brain Motion of a Novel Anthropometric Test Dummy Head using 6DOF Sensors

Hiroki Yamamoto
Tokyo Institute of Technology in Japan

Y. Miyazaki [1], S. Awamori [1], A. Kokeguchi [2], I. Amamori [2], K. Yoshii [2]
[1] Tokyo Institute of Technology, [2] Joyson Safety Systems Japan

INTRODUCTION

More than a million people die from road traffic accidents a year worldwide. Traumatic brain injury is the primary cause of death in road traffic accidents. Performance evaluation for overall vehicle safety and evaluation of safety devices are based on the use of anthropometric test devices (ATDs).

However, these heads, which have no moving parts representing the soft tissues and no special instrumentation to capture the motion of the brain, do not incorporate actual human geometry. Some previous studies have suggested that such instrumentations be installed in actual ATD heads used for testing. The authors in [1] used a simplified model using acrylic aspherical calvarium and a gelatin brain, but no dura, falx, or tentorium. All these previous models lack a complete 3D representation of the shapes of the actual human head and brain in its entirety. The authors in [2] developed a novel ATD head based on actual human anatomy and biomimetic materials that are capable of direct measurement and visualization of intracranial brain motion in frontal sled tests by using stereo cameras. However, this method is sensitive to lighting conditions and objects casting shadows. It is also impossible to capture the markers on the brain and skull when airbags enter the space between the cameras and ATD head.

Therefore, the objectives of this study are to develop a novel ATD head incorporating not only skull-brain structures, robust instrumentation, but also 6 degrees of freedom (DOF) measurement systems regardless of the experimental conditions, and a method to calculate the skull-brain relative motion from the data of the 6DOF sensors. Following that, in order to determine whether it is possible to measure the intracranial brain motion easily and continuously using 6DOF sensors on the fundamental head impact experiments, we conducted occipital head impact tests.

METHODS

The following requirements were set as design targets for the model: 1) the anatomical structure of the model should be based on the actual human head; 2) the new ATD head should be usable as a replacement for existing ATD heads such as the Hybrid III; and 3) it should be able to easily and continuously measure the skull-brain relative displacement regardless of the experimental conditions.

Novel ATD Head with 6DOF Sensors

A novel ATD head was constructed based on the geometry obtained from adult human male CT and MRI images, as in [2], and a detailed CAD model is shown in Figure 1. This physical model consists of a silicone gel brain, polycarbonate skull, silicon rubber skin, polyurethane tentorium, and falx. The brain physical model, which consists of the right and left cerebrum, tentorium, and falx were inserted into the skull model, and the intracranial space was suffused with water as cerebrospinal fluid to allow relative displacement between the skull and brain. A neck mounting plate, that has the exact same shape of a mounting plate as that of the Hybrid Ⅲ, was attached to the ATD head on the Hybrid Ⅲ neck. The 6DOF sensors (DTS 6DX PRO) were installed in the nasal bone part and the right and left cerebrum (Figure 2), which would be possible to measure the relative skull-brain displacement easily and continuously regardless of the experimental conditions. The two sensors for the brain were covered with a silicone sealant and a box made of acrylonitrile butadiene styrene to mimic an equivalent density to the surrounding silicone gel brain. The assembled ATD head is shown in Figure 3. Moreover, the tendency of the brain motion of the ATD head due to impacts showed a strong correlation with the finite element (FE) model validated against a cadaver study. However, as this physical model does not have the meninges, the relative motion of the brain with respect to the skull was approximately three times

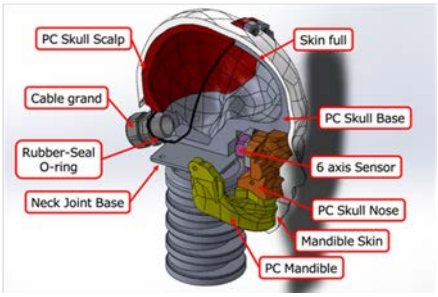

Figure 1. CAD model

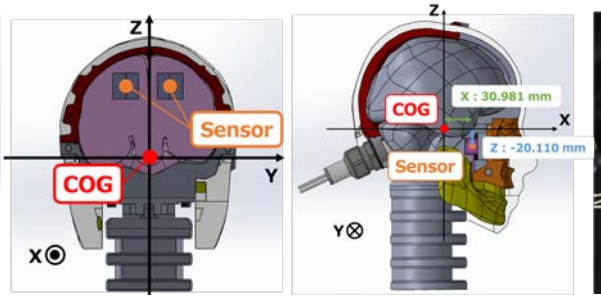

(a) *(b)*

Figure 2. Sensors and COG position and reference coordinate system

Figure 3. Assembled ATD head

larger than that of the FE model.

Measurement of Intracranial Brain Motion

The center of gravity (COG) of the head is separated from the location of the 6DOF sensor in the nasal bone. Material properties were assigned to the CAD model, and the location of the COG of the head was estimated. The following equation was used to convert the captured data at the 6DOF sensor location to the COG location.

$$\boldsymbol{a_{cog}} = \boldsymbol{a_{skull}} - \ddot{\boldsymbol{\theta}} \times \boldsymbol{r_1} - \dot{\boldsymbol{\theta}} \times (\ddot{\boldsymbol{\theta}} \times \boldsymbol{r_1}), \quad (1)$$

where $\boldsymbol{a}$, $\dot{\boldsymbol{\theta}}$, and $\ddot{\boldsymbol{\theta}}$ are the linear acceleration, angular velocity, and angular acceleration vector, respectively, and $\boldsymbol{r_1}$ is the position vector from the COG to the sensor. Moreover, the coordinates of the two sensors in the brain part should be transformed for every sampling so that they are parallel to the reference coordinate system. According to Rodrigues' rotation formula, the coordinate transformation is calculated as

$$\boldsymbol{a_{brain}} = \boldsymbol{E_t a'_{brain}}, \boldsymbol{\omega_{brain}} = \boldsymbol{E_t \omega'_{brain}},$$
$$\boldsymbol{E_{t+1}} = \boldsymbol{R E_t} \quad (2)$$
$$\boldsymbol{R} = \boldsymbol{I} + [\boldsymbol{n}\times] sin\theta + [\boldsymbol{n}\times]^2 (1 - cos\theta),$$
$$\theta = \Delta t \|\boldsymbol{\omega_{brain}}\|, [n_1\ n_2\ n_3]^T = \frac{\boldsymbol{\omega'_{brain}}}{\|\boldsymbol{\omega'}_{brain}\|},$$

where $\boldsymbol{I}$ is an identity matrix, $\boldsymbol{n}$ is a skew-symmetric matrix, and Δt is the sampling duration time. The drift errors are interpolated after calculating the velocity and position in which the acceleration is time-integrated.

Occipital Head Impact Tests

To determine whether it was possible to measure the intracranial brain motion easily and continuously on the fundamental head impact tests, we conducted occipital head impact tests. Additionally, in order to analyze human tolerance levels for bridging vein damage, we reconstructed the cadaver experiments [3] with two measurement methods. On one hand, the skull and brain markers were tracked by using two high-speed cameras at 1000 fps with LED lights as in [2]. On the other hand, the skull-brain relative displacement was continuously measured using two 6DOF sensors in the brain at 10 kHz. A Hybrid III AM50 dummy was used for the experiments. The Hybrid III head was replaced with our novel ATD head. An impactor (15.6 kg) was collided with the ATD occipital head. The linear acceleration and angular velocity in the bosal bone and right and left cerebrum were measured. We conducted 48 occipital impact tests by changing 14 impact energies. The data from the sensors and angular acceleration differentiated sensor's angular velocity were filtered by CFC 180 and CFC 60.

RESULTS

Figure 4 shows the maximum and minimum values of the relative skull-brain displacement measured by tracking the markers and calculated relative displacement values (1-2). The yellow (left cerebrum) and purple (right cerebrum) lines denote relative displacements calculated from the sensors within the corridor of the displacements measured by cameras. The relationship of the peak change of the relative skull-brain displacement between the brain surface at the marker position and brain inside at the sensor position is shown in Figure 5. There was a strong linear correlation between these values.

DISCUSSION

According to the reconstructed cadaver study results, bridging vein damage occurred in the cases when the peak change of angular velocity around the y-axis of the cadaver heads exceeded 40 rad/sec [3]. The relationship between the peak change between the angular velocity and the relative displacement at the sensor is shown in Figure 6. When the angular velocity around the y-axis was 40 rad/sec, the relative

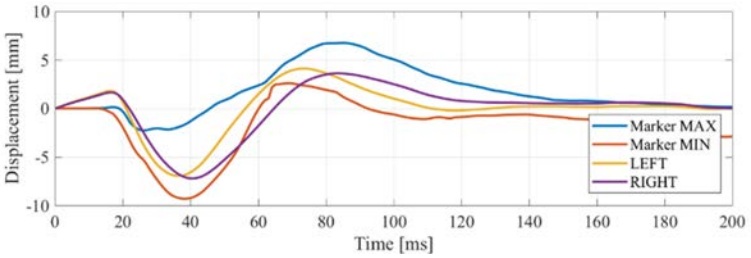

Figure 4. Maximum and minimum values of the skull-brain relative displacement and the calculated values from the sensors data

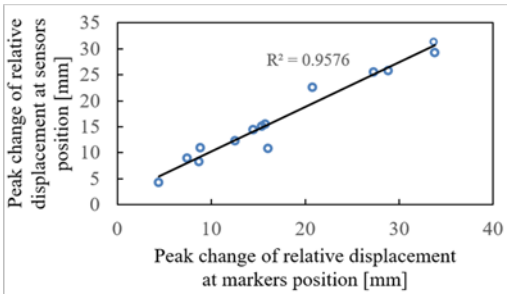

Figure 5. Relationship of peak change of relative displacement between brain surface and inside

displacement at the sensor was 33.2 mm. Note that the brain motion of this physical model is approximately three times larger than that in an actual human or FE model. However, the results showed a strong linear correlation; therefore, our model can be used for evaluating the risks of bridging vein damage.

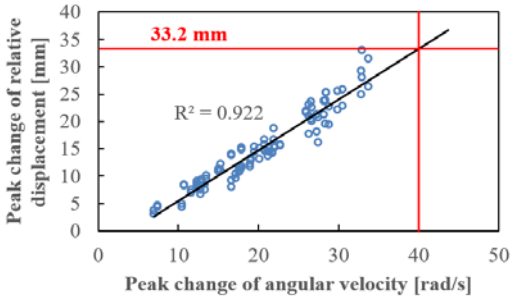

Figure 6. Relationship of peak change between angular velocity around y-axis and relative displacement

CONCLUSION

By measuring the linear acceleration and angular velocity in the brain with 6DOF sensor measurement systems, we evaluated the brain motion directly and easily without stereo cameras. We showed the potential of the novel ATD head for use in camera-less experimental conditions such as the sport helmets test. In crash tests, the duration of impact would be longer, which means it may be necessary to prepare a data assimilation system for mitigating drifting errors. For example, the angle of the brain sensors will be estimated from the acceleration data, and these values will be used for the true values on the extended Kalman filter. The biofidelity of the ATD head can also be improved by modeling the meninges. It is difficult to reproduce the complex structure of the Pia-Arachnoid complex. Many aspects of the interface between the brain and skull are not clear. However, we hypothesize that covering a silicone gel brain with a surrogate object, as a pia mater is one solution. It may not improve biofidelity, but we are sure that it will lead to improved handling properties and robust instrumentation.

NOVELTY/TRAFFIC SAFETY IMPLICATIONS

Our novel ATD head incorporates skull-brain structures based on an actual human head and makes it possible to measure the relative brain-skull displacement easily and continuously without stereo cameras. We should consider the limitation that the brain motion of our physical model is larger than that in an actual human or the FE model. However, there is a strong linear correlation with an actual human or FE model. Moreover, the 6DOF sensor measurement systems worked well compared to the optical methods using cameras. This will allow us to develop and evaluate safety devices regardless of hidden head markers from the cameras during airbag and sport helmet tests, among others.

REFERENCES

[1] Cheng J, Howard I and Rennison M. Study of an infant brain subjected to periodic motion via a custom experimental apparatus design and finite element modelling. *Journal of Biomechanics*, vol. 43, no. 15, pp. 2887-2896, 2010.

[2] Miyazaki Y, Railar A, Awamori S, Kokeguchi A, Amamori I, Katagiri M and Yoshii K, “Intracranial brain motion measurement in frontal sled test by using a new anthropometric test dummy head capable of direct brain motion evaluation and visualization,” *International Research Council on Biomechanics of Injury*, pp 284-295, 2017

[3] Depreitere B, Van Lierde C, Sloten JV, Van Audekercke R, Van der Perre G, Plets C and Goffin J. “Mechanics of acute subdural hematomas resulting from bridging vein rupture,” *Journal of Neurosurgery*, vol. 104, no. 6, pp. 950-956, 2006.

NOVEL EXPERIMENTS TO ASSESS STIFFNESS RESPONSE OF LUMBAR SPINE IN FLEXION

Kalle Chastain
Center for Applied Biomechanics, University of Virginia

Watson Spivey[1], David Moreau[1], Brian Overby[1], Bronislaw Gepner[1], Jason Forman[1], Jason Hallman[2], Jason Kerrigan[1]
[1]Center for Applied Biomechanics, University of Virginia
[2]Toyota Motor Eng. & Mfg. North America

INTRODUCTION

Highly automated vehicles may enable an increase of non-traditional seating positions chosen by vehicle occupants, potentially including a higher prevalence of reclined riding postures. In highly reclined postures, novel lap belt design strategies may minimize the risk of submarining. However, increased pelvis restraint may increase compressive loads in the lumbar spine which~~, superimposed~~, superimposed with flexion moment, may place the lumbar spine at greater risk of injury compared to upright postures. In addition, the relationship between pelvis and upper body kinematics is likely to be influenced by the bending stiffness, and specifically that stiffness under superimposed axial compressive load, of the lumbar spine [1-3]. Unfortunately, little data exists in the literature to assess biofidelity of human body model (HBM) lumbar spines subjected to this combined loading, which will be critical to predictive injury risk assessments for reclined occupants. Past studies of whole lumbar spine loading with compression have resulted in undesirable buckling [4,5]. Further efforts were taken to reduce buckling through implementation of a follower load [6,7]. The goal of this study was to characterize the stiffness response of the lumbar spine during flexion with and without a combined axial compressive loading using a novel displacement and follower load mechanism.

METHODS

In this study, post-mortem human surrogate (PMHS) whole lumbar spines (male, 40.3±11.8 years, 25.7±3.79 BMI) were tested with a 6 degree-of-freedom (DOF) robotic test device and linear actuators. The robot was used to apply desired 6-DOF motion to the specimen, while actuators were used to apply the follower load (Figure 1). A follower load is a technique used to direct the compression load along the curvature of the spine, thus constraining off-axis motions, and simulating the stabilizing effect of lumbar musculature [8,9]. Some designs include vertebral harnesses containing slip rings to accommodate cables following the local spine curvature [9,10]. In this study, the surrogate vertebrae were each outfitted with rigidly affixed, 3D-printed collars containing motion-tracking markers. The actuator cables were fed through each collar and attached to the bottom potting cup. The collars enabled anterior/posterior adjustment of the cables relative to the vertebral bodies in order to find the local center of rotation at each level. Care was taken to adjust the cables such that any residual moment during pure axial compression was minimized. The actuators were programmed to maintain a pre-determined tension force, while the robot was allowed to move and pre-compress the spine to the desired level of follower load. With the follower load in place, the robot was used to apply the desired flexion motion. These motions were defined within a local joint coordinate system (JCS) at the L4-L5 level established during initial setup.

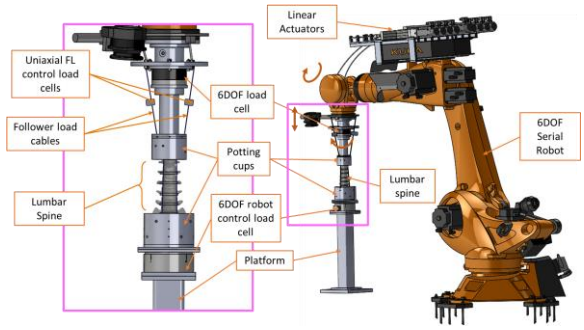

Figure 2. Schematic showing a structural characterization experiment with a lumbar spine PMHS.

Individual experiments were performed to characterize the response of the spine under pre-defined flexion motion. Each spine was tested without follower load, a mid-level (900N) and a high-level (1800N) follower load. Tests were performed in both position- and force-control, with load maintained below injurious levels. The spine was rotated in position-control to a desired flexion rotation while the robot was instructed in force-control to adjust movements such that anterior/posterior shear was minimized in order to record pure flexion moment. Afterward the spine was held in place to observe stress-relaxation response then returned to a neutral position. 6-DOF force and moment, precise robot position, and 3D-motion tracking data for each vertebra were recorded. The moments were measured at the bottom load cell and transformed to the JCS located in the L4-L5 intervertebral disc.

RESULTS

A non-linear response was observed in the cases without follower load (Figure 2) and a more linear response was seen in the mid-level follower load (Figure 3) and high-level follower load cases (Figure 4).

Additionally, in the follower-load cases, there is a residual moment seen at the beginning of the cycle for each specimen. This was a result of the minimized value of residual moment we were able to achieve during initial setup of the follower load. Similarly there is a reduction in moment at the peak of flexion rotation.

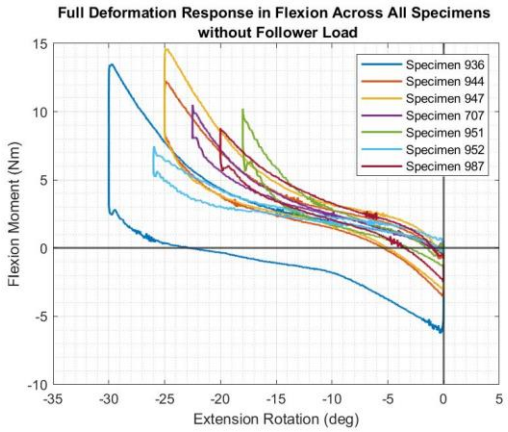

Figure 2. Deformation responses across all specimens tested in flexion without a follower load

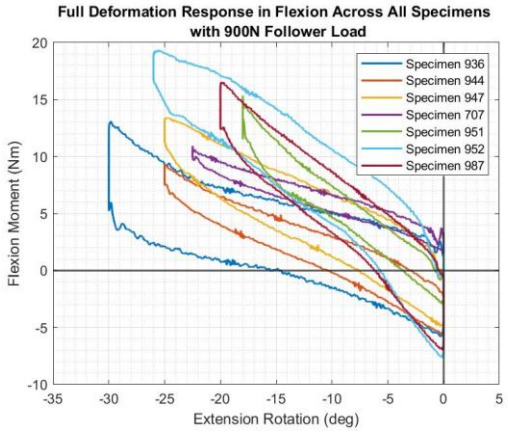

Figure 3. Deformation responses across all specimens tested in flexion with a 900N mid-level follower load applied

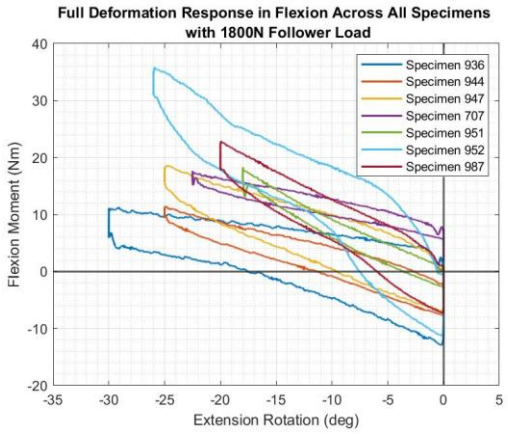

Figure 4. Deformation responses across all specimens tested in flexion with an 1800N high-level follower load applied

DISCUSSION

The stiffness response of the lumbar spine was affected by the introduction of axial compression from a follower load. One possible explanation for the difference in behavior of cases with and without follower load is the addition of axial compression via follower load released tension on the posterior longitudinal ligament (PLL) causing the spine to become less stiff in larger rotations compared to the non-follower load cases.

In the cases without follower load, the rate of stiffness is higher initially, decreases before increasing again until the peak rotation angle resulting in an S-shaped curve. One explanation for this initial stiffness rate is the result of residual anterior shear during the movement of the robot. This shear is then corrected by the robot to a pure flexion moment resulting in the flatter region of the cycle. This shear correction combined with tissue relaxation could also explain the moment reduction seen at peak rotation.

CONCLUSION

This study sought to characterize the lumbar spine stiffness response in the flexion direction with and without the inclusion of axial load through a follower load mechanism. Motion and loads were characterized in the flexion direction and stiffness responses were created for the use of biofidelity assessment of HBMs.

NOVELTY/TRAFFIC SAFEY IMPLICATIONS

With the increased likelihood of non-traditional seating postures assumed to accompany the future availability of highly automated vehicles, injury patterns of frontal crashes may include more injuries to the lumbar spine due to combined flexion and axial loading. To the extent of the authors' knowledge, this is the first study to compare the mechanical response of the lumbar spine in flexion with and without the inclusion of axial compression via follower load. With the addition of this data set, assessment of biofidelity of existing HBMs can begin in order to better predict human response to crashes in these new driving conditions.

ACKNOWEDGEMENTS

The authors would like to thank the Toyota Collaborative Safety Research Center (CSRC) for their continued support throughout this project and to the families of the donors represented in this study.

REFRENCES

[1] Rawska, K, Gepner, BD, Kerrigan, JR, et al. (2019) Submarining Sensitivity across Varied Anthropometry in Autonomous Driving System Environment. Proceedings of AAAM, Madrid, Spain, October 15-18.

[2] Gepner, BD, Draper, D, Mroz, K, et al. (2019) Comparison of Human Body Models in Frontal Crashes with Reclined Seatback. Proceedings of the International Research Council on the Biomechanics of Impact (IRCOBI), IRC-19-44. Florence, Italy. September 11-13.

[3] Richardson, R, Donlon, J. P., Chastain, KL, et al. (2019). Test methodology for evaluating the reclined seating environment with human surrogates. In *26th ESV Conference. In press. Eindhoven, Netherlands*.

[4] Duma, S, Kemper, A, McNeely, DM, et al. (2006) Biomechaical response of the lumbar spine in dynamic compression. Biomed. Sci.Instrum 42: 476-481.

[5] Demetropoulos, CK, Yang, KH, Grimm, MJ, et al. (1999). High rate mechanical properties of the Hybrid III and cadaveric lumbar spines in flexion and extension (No. 99SC18). SAE Technical Paper.

[6] Curry, WH, Pintar, FA, Doan, NB, et al. (2016) Lumbar spine endplate fractures: biomechanical evaluation and clinical considerations through experimental induction of injury. Journal of Orthopaedic Research 34, no. 6: 1084-1091.

[7] Yoganandan, N, Arun, MWJ, Stemper, BD, et al. (2013) Biomechanics of human thoracolumbar spinal column trauma from vertical impact loading. AAAM 57: 155.

[8] Slosar Jr, PJ, Patwardhan, AG, Lorenz, M, et al. (1995) Instabilityof the lumbar burst fracture and limitations of transpedicular instrumentation. Spine 20, no. 13:1452-1461.

[9] Rohlmann, A, Neller, S, Claes, L, et al. (2001) Influence of a follower load on intradiscal pressure and intersegmental rotation of the lumbar spine. Spine 26, no. 24: E557-E561.

[10] Patwardhan, AG, Havey, RM, Meade, KP, et al. (1999) A follower load increases the load-carrying capacity of the lumbar spine in compression. Spine 24, no. 10: 1003-1009.

Development of an upper cervical spine model for use in an omnidirectional surrogate neck

Sarah Romani
University of British Columbia

Graham Fonseca, Peter Cripton
University of British Columbia

INTRODUCTION

Anthropomorphic test devices (ATDs) or crash test dummies are an important tool in the development and testing of safety equipment for automotive applications. ATD necks control the motion of the head; they are designed for a specific loading scenario and are typically biofidelic only in that application [1][2]. There is no single surrogate appropriate for the multiplane loading that often occur. The long-term goal of this project is to create an omnidirectional ATD neck that is biofidelic in headfirst impacts, as well as in head impacts and inertial loading in the transverse plane. We plan to accomplish this by replicating the geometry and mechanical properties of key anatomical structures in the neck.

Here we report on our approach to generating a surrogate of the anatomically complex upper cervical spine (UCS) consisting of the C0-C2 vertebra. It and enables the majority of the cervical spine's axial rotation, making it a critical structure in the determination of head motion [3]. Thus, it is important that this region is faithfully replicated in the proposed surrogate neck. In many of the existing ATDs, a pin joint replicates the UCS, allowing only movement in the sagittal plane [3][4].

METHODS

This surrogate neck must be able to withstand greater than injurious physiological loads and must match the intervertebral kinematics in flexion-extension, lateral bending and axial rotation.

The two main structures that we replicated in this model are the vertebra and the ligaments as they are the main limiters of motion, and prescribe the motion of one vertebra with respect to those adjacent[3].

Model development

Vertebral surrogate

For the construction of the vertebra, we obtained CT scans from a 31-year-old male with no cervical spine pathologies from Vancouver General Hospital through a collaboration with the UBC Dept. of Orthopaedics Spine Surgery Group. These were segmented using the Analyze software (Biomedical Imaging Resource, Mayo Clinic). Scans were smoothed using the Meshmixer software (Autodesk) and transferred to CAD files. These files were modified to include attachment points for ligaments and to the test apparatus and were then 3D printed in PLA Figure 1.

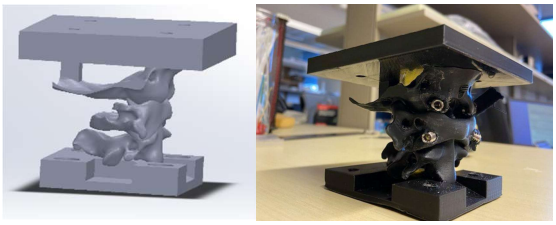

Figure 1: CAD model (left) and 3D printed (right) C0-C2 segments

The CT scans were taken supine; it has been shown that the sagittal alignment of the spine varies between supine and seated positions [4]. Because of this, we realigned vertebrae in the sagittal plane based on a series of radiographic markers. The markers used included the angle of the McRae line from the horizontal [7] and the base of C2 [8]. For translational alignment, we used two clinical markers, the Harris rule of 12 and the posterior axial dens interval [9].

Ligament surrogate

As it is not practical to replicate the large number of ligaments in this section of the neck, the transverse and alar ligaments were replicated first as they are believed to be the most deterministic to the kinematics of the region[5]. The alar ligament is a paired ligament that runs from the sides of the upper third of the dens to the interior surface of the occipital condyles[6]. The transverse ligament passes between the tubercles located on either side of the vertebral foramen[7]. The attachment points generated on the vertebral models for these ligaments were based on these anatomic

landmarks and then checked to ensure they were within one standard deviation of the average placements as measured by Panjabi[7].

The stiffness of candidate materials was tested in uni-axial tension on an Instron materials testing machine and compared to the stiffness of cadaveric ligaments at similar strain rates. The stiffness ranges used were the maximum and minimum of the standard deviations of the results reported by Panjabi and Mattucci[8], [9]. We selected a cotton webbing for the surrogate ligament material for this prototype iteration.

Table 1: Stiffness of surrogate ligament material

Ligament	Ligament length (mm) [8]	Stiffness range (N/mm) [8], [9]	Surrogate ligament stiffness (N/mm)
Alar ligament	11.2	70.7-270	167.48
Transverse ligament	18	120-218	90.81

Testing

For testing, a custom spine machine built in our lab (Figure 2) was used to apply pure moments in flexion-extension, lateral bending and axial rotation to the specimen [10]. Markers were attached to each of the vertebrae, and their movements tracked using the Optotrak motion analysis system (Northern Digital, Waterloo, Canada). In this way, the applied moments and corresponding movements of the vertebrae can be recorded and evaluated. The first metric that we used to compare results to those from cadaveric specimens is range of motion. In future analyses, the neutral zone and centers of rotation will be added.

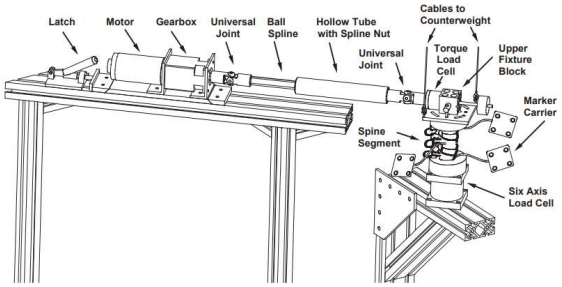

Figure 2: Custom spine machine [10]

RESULTS

Preliminary results from the generated rotation/moment curve of the C0-C2 segment in flexion-extension are shown in orange in Figure 3 plotted along with rotation/moment curves from other studies using cadaveric specimens. The maximum range of motion in extension is within the range of the cadaveric results presented, but the range of motion in extension notably exceeds it.

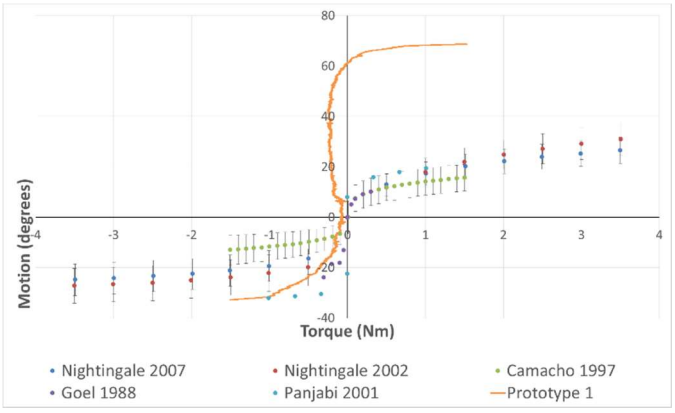

Figure 3:Rotation/moment curve under flexion-extension [11]–[14]

The corresponding rotation/moment curve for the surrogate UCS in lateral bending is shown in orange in Figure 4 below. The range of motion in both directions here greatly exceeds the cadaveric ranges of motion.

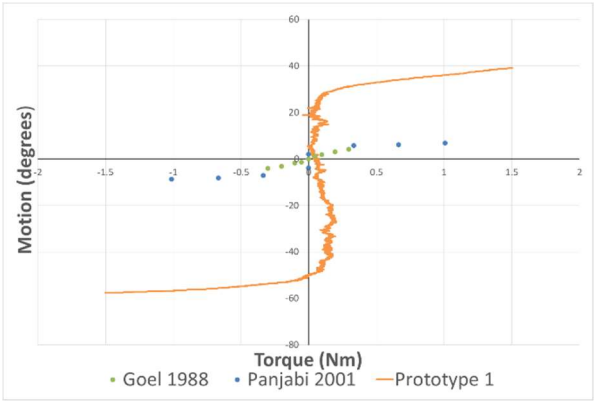

Figure 4:Rotation/moment curve under lateral bending[13], [14]

DISCUSSION

Excessive flexion

As is seen in Figure 3, the range of motion in flexion markedly exceeded the expected results. In the lateral bending tests, we observed that the segment flexed considerably which may have contributed to this increased range of motion also seen in lateral bending.

We think that by limiting the flexion, the resultant range of motion will be much closer to the expected results in both flexion-extension and lateral bending.

The nuchal ligament was not one of the ligaments replicated in this prototype and is believed to be a limiter of flexion[15]. It spans the cervical spine from C7 to occiput and is the most posterior structure of the

cervical spine. As a result, it is well-positioned to limit flexion. By replicating the action of this ligament, we hypothesize we can limit the excessive flexion we are seeing. CVJ flexion limiters have been implemented in muscle force replicators on cadaveric spines as well as in crash test dummies and will be implemented in subsequent iterations of this prototype [16], [17].

CONCLUSION

The development of an upper cervical spine surrogate that matches the kinetic and kinematic response of cadaveric specimens represents an important step in the eventual construction of a full biofidelic omnidirectional surrogate neck. The data collected in the testing of this first-generation prototype gives important information that can be used in the next generation of prototypes. Such a neck could then be used to develop and evaluate safety equipment for a wide range of settings, including automotive.

NOVELTY/TRAFFIC SAFETY IMPLICATIONS

This project is novel in its approach to the development of a surrogate cervical spine. By replicating the geometry of the vertebrae of a specific person, we hope to be one step closer to developing a surrogate neck that represents a real person rather than a hypothetical average geometry. This approach could be extended to a wide range of demographics.

Head and neck injuries are common in vehicle accidents, particularly rollover crashes[18]. In which the loading scenarios experienced, from the initial impact and roll to the impact of the head to the roof, are complex. To the best of our knowledge, there is not yet an ATD that has been shown to be biofidelic in rollover applications[19]. Having an omnidirectional surrogate neck such as the one proposed here could be used in ATDs to aid in the effective testing and development of safety equipment. This, in turn, could one day help to reduce the frequency and severity of these types of injuries.

ACKNOWLEDGEMENTS

We would like to acknowledge Lani Reichl and Dr. Brian Kwon for their help with obtaining the CT scans.

REFERENCES

[1] J. Davidsson, P. Lovsund, K. Ono, M. Y. Svensson, and S. Inami, "A Comparison of Volunteer, BioRID P3 and Hybrid III Performance in Rear Impacts," *J. Crash Prev. Inj. Control*, vol. 2, no. 3, pp. 203–220, 2007.

[2] G. Shaw, "Biofidelity Evaluation of the Thor Advanced Frontal Crash Test Dummy," *IJCrash*, vol. Montpellie, p. 2000, 2010.

[3] A. J. Lopez, J. K. Scheer, K. E. Leibl, Z. A. Smith, B. J. Dlouhy, and N. S. Dahdaleh, "Anatomy and biomechanics of the craniovertebral junction," *Neurosurg. Focus*, vol. 38, no. 4, p. E2, 2015.

[4] F. Sato *et al.*, "Analysis of the alignment of whole Spine in automotive seated and supine postures using an upright open MRI system," *Int. J. Automot. Eng.*, vol. 7, no. 1, pp. 29–35, 2016.

[5] C. B. Lumenta, C. Di Rocco, J. Haase, and J. J. A. Mooij, *European Manual of Medicine — Neurosurgery*, vol. 24, no. 1–2. 2012.

[6] P. G. Osmotherly, D. A. Rivett, and S. R. Mercer, "Revisiting the clinical anatomy of the alar ligaments," *Eur. Spine J.*, vol. 22, no. 1, pp. 60–64, 2013.

[7] M. M. Panjabi, T. R. Oxland, and E. H. Parks, "Quantitative anatomy of cervical spine ligaments. Part I. Upper cervical spine," *Journal of Spinal Disorders*, vol. 4, no. 3. pp. 270–276, 1991.

[8] M. M. Panjabi, J. J. Crisco, C. Lydon, and J. Dvorak, "The mechanical properties of human alar and transverse ligaments at slow and fast extension rates," *Clin. Biomech.*, vol. 13, no. 2, pp. 112–120, 1998.

[9] S. F. E. Mattucci, J. A. Moulton, N. Chandrashekar, and D. S. Cronin, "Strain rate dependent properties of human craniovertebral ligaments," *J. Mech. Behav. Biomed. Mater.*, vol. 23, pp. 71–79, 2013.

[10] D. J. Goertzen, C. Lane, and T. R. Oxland, "Neutral zone and range of motion in the spine are greater with stepwise loading than with a continuous loading protocol. An in vitro porcine investigation," *J. Biomech.*, vol. 37, no. 2, pp. 257–261, 2004.

[11] R. W. Nightingale, B. A. Winkelstein, K. E. Knaub, W. J. Richardson, J. F. Luck, and B. S. Myers, "Comparative strengths and structural properties of the upper and lower cervical spine in flexion and extension," *J. Biomech.*, vol. 35, no. 6, pp. 725–732, 2002.

[12] D. L. Camacho, R. W. Nightingale, J. J. Robinette, S. K. Vanguri, D. J. Coates, and B. S. Myers, "Experimental flexibility measurements for the development of a computational head-neck model validated for near-vertex head impact," *Stapp Car Crash Conference Proceedings*, no. P-315. pp. 473–486, 1997.

[13] V. K. Goel, C. R. Clark, K. Gallaes, and Y. K. Liu, "Moment-rotation relationships of the ligamentous occipito-atlanto-axial complex," *J. Biomech.*, vol. 21, no. 8, 1988.

[14] M. Panjabi, R. J. Brand, and A. 3rd White, "Mechanical Properties of the Human Cervical Spine as Shown by Three-Dimensional Load – Displacement Curves," *J. Bone Joint Surg. Am.*, vol. 58, no. 5, pp. 642–652, 2001.

[15] K. Takeshita, E. T. K. Peterson, D. Bylski-austrow, A. H. Crawford, and K. Nakamura, "The Nuchal Ligament Restrains Cervical Spine Flexion," *Spine (Phila. Pa. 1976).*, vol. 29, no. 18, pp. 388–393, 2004.

[16] P. C. Ivancic, M. M. Panjabi, S. Ito, P. A. Cripton, and J. L. Wang, "Biofidelic whole cervical spine model with muscle force replication for whiplash simulation," *Eur. Spine J.*, vol. 14, no. 4, pp. 346–355, 2005.

[17] E. Spittle, B. W. Shipley, and I. Kaleps, "Hybrid III and Hybrid III Dummy Neck Proeprties for Computer Modeling," *Air Force Syst. Command. Wright-Patterson Air Force Base, Ohio*, pp. 1–138, 1992.

[18] C. W. Roberts, J. Toczyski, and J. R. Kerrigan, "Cervical spine injury in rollover crashes: Anthropometry, excursion, roof deformation, and ATD prediction," *Clin. Biomech.*, vol. 64, no. March 2018, pp. 42–48, 2019.

[19] Q. Zhang *et al.*, "Occupant Kinematics in Laboratory Rollover Tests: ATD Response and Biofidelity," *Stapp Car Crash J.*, vol. 58, no. November, pp. 317–360, 2014.

FEMALE AND MALE VOLUNTEER KINEMATICS DURING RELAXED AND BRACED PRE-CRASH BRAKING EVENTS

Hana Chan[1]
[1] Virginia Tech Center for Injury Biomechanics, Blacksburg, VA

Devon L. Albert[1], F. Scott Gayzik[2], Andrew R. Kemper[1]
[1] Virginia Tech Center for Injury Biomechanics, Blacksburg, VA
[2] Wake Forest University Center for Injury Biomechanics, Winston-Salem, NC

INTRODUCTION

In model year 2016, over half of United States vehicle series offered some type of frontal crash prevention system, such as autonomous emergency braking (AEB), as an optional safety feature [1]. Twenty automakers, representing 99% of all United States automakers, have committed to making AEB (and forward collision warning) a standard feature on all new passenger vehicles by 2022 [1]. While these active safety systems can reduce the number and severity of injuries in frontal motor vehicle collisions (MVCs) by decreasing the incidence and severity of collisions, they can also displace occupants out of position during a pre-crash event. This is especially important to consider because occupant safety during a crash event is evaluated using an idealized driving position. Moving out of this idealized driving position prior to impact can influence the performance of vehicle restraints and/or lead to undesirable interactions with the vehicle interior in a subsequent frontal MVC, resulting in potentially different injury risks and outcomes [2].

Due to the low severity and long duration of pre-crash braking events, there is sufficient time for muscle activation to affect occupant position prior to impact. To address this, computational human body models (HBMs) have incorporated active musculature to evaluate the influence of occupant displacements during pre-crash events on vehicle safety performance during a subsequent frontal MVC [3]. However, in order to accurately represent the response of live occupants, HBMs must be validated with appropriate volunteer data. Previous studies have investigated volunteer occupant kinematics during pre-crash braking events [4-5] and the effects of pre-impact bracing during low-speed frontal sled tests [6]. However, few studies have included small female volunteers and compared the differences to males [7], which precludes the ability to properly validate female active muscle models and assess differences between sexes.

Therefore, the objective of this study was to quantify occupant kinematics for both small female and mid-size male volunteers during relaxed and braced pre-crash braking events, and evaluate the differences in occupant kinematics between muscle conditions and sexes.

METHODS

Three approximately 5th percentile female volunteers and three approximately 50th percentile male volunteers (Table 1) each experienced two frontal sled tests that simulated a pre-crash braking event (1.1 g peak acceleration, 0.44 second duration).

Table 1. Volunteer demographics and anthropometry.

Sex	Age (years)	Height (cm)	Weight (kg)
Female	26.0 ± 1.0	159.5 ± 4.6	51.2 ± 0.9
Male	23.7 ± 2.5	174.8 ± 1.6	78.1 ± 3.0

For each test, subjects were either relaxed or braced prior to the impulse. For the relaxed tests, subjects were instructed to remain relaxed, face forward, and watch a monitor playing a show or movie (Figure 1). They were then told that the pulse would be triggered randomly in the next several minutes. When subjects appeared focused on the monitor, relaxed, and relatively still, the pulse was triggered out of sight from the subjects so they were unaware of when the test would begin. For the braced tests, a countdown was used to instruct subjects when to begin bracing (two seconds prior to impulse) and when the test would start. When bracing, subjects were instructed to push on the steering wheel and foot pedals with their upper and lower extremities, respectively, and the seat back with their torso as if they were anticipating a crash event.

All tests were performed on a custom rigid buck and mini-sled powered by a pneumatic piston. The test buck was modified with spacers on the steering column, seat back, seat pan, and foot pedal surfaces for female subjects to maintain consistent resting joint angles with male subjects.

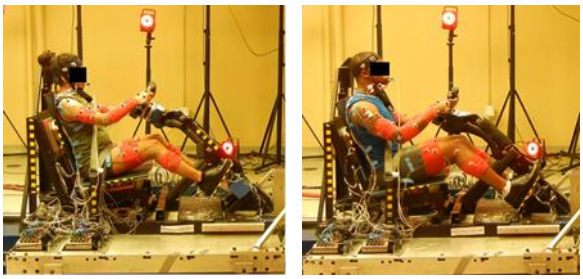

Figure 1. Female (left) and male (right) subjects seated in test buck prior to start of a relaxed test.

A Vicon motion capture system was used to quantify 3D kinematics of the subjects and test buck (1000 Hz sampling rate). Retro-reflective markers were attached to the test buck and to the subjects at key anatomical locations: head CG, C7, shoulders (acromion), elbows, hips (greater trochanter), and knees. Marker trajectories relative to the test buck were calculated by subtracting buck motion. Marker trajectories were also converted to the SAE J211 sign convention. Peak *x* (+ forward) and *z* (+ downward) marker excursions were determined from marker trajectory data relative to initial marker positions at the start of the test, and then compared between muscle conditions and sexes. All testing was approved by the Virginia Tech Institutional Review Board.

RESULTS

Pre-impact bracing affected all peak marker excursions for both sexes. Specifically, bracing decreased peak forward head, C7, shoulder, elbow, hip, and knee excursions (Figure 2Figure ***3***). Bracing also decreased peak upward C7 and knee excursions. For males, bracing decreased their peak downward head and elbow excursions.

Subject sex affected peak marker excursions differently between muscle conditions. Males had greater peak forward head, C7, shoulder, and elbow excursions than females when relaxed (Figure 2). When bracing, there was little difference between female and male peak forward excursions at all anatomical locations except for the head, where males had greater peak forward excursions (Figure 3).

DISCUSSION

Overall, pre-impact bracing decreased peak forward marker excursions for both sexes. Comparisons between female and male occupant kinematics suggest that while males had greater peak forward excursions at all anatomical locations compared to females when relaxed, they responded more similarly when braced.

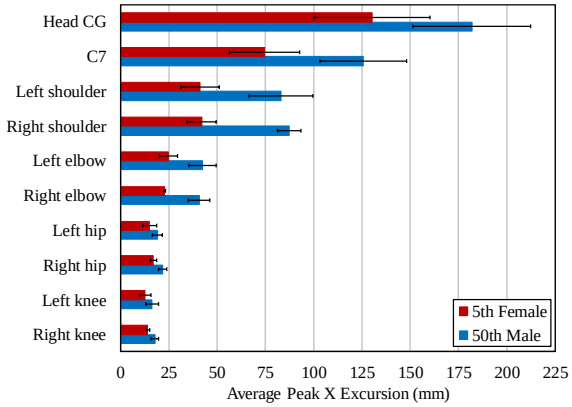

Figure 2. Average peak forward excursions for relaxed tests.

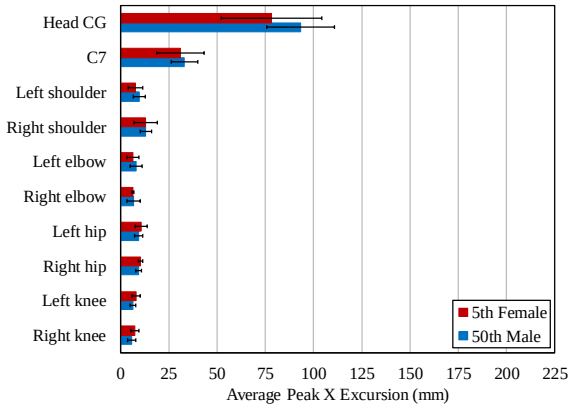

Figure 3. Average peak forward excursions for braced tests.

Both the female and male volunteers' heads moved forward considerably, even when bracing. The females' heads moved forward 11.4-16.5 cm when relaxed (Figure 4) and 5.5-10.6 cm when braced (Figure 5). The males' heads moved forward 14.9-20.9 cm when relaxed (Figure 4) and 7.3-10.5 cm when braced (Figure 5). This large degree of head movement is important to note because it occurred during an acceleration pulse which was designed to be similar to an autonomous braking event. This could have implications for occupant safety when evaluating the effectiveness of active safety systems such as AEB. During a pre-crash scenario where AEB is activated, occupants can displace forward and out of position, decreasing the distance between the occupant and vehicle interior. In the event that AEB does not avoid a frontal collision, this could potentially decrease restraint effectiveness and lead to undesirable interactions with the steering column or airbag in the event of a subsequent MVC.

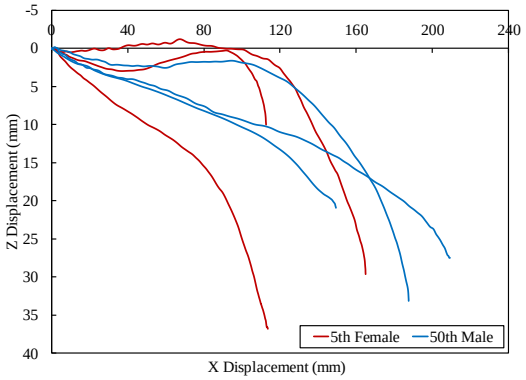

Figure 4. Sagittal plane head excursions for relaxed tests.

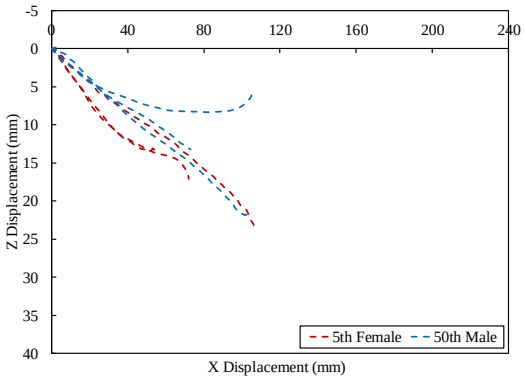

Figure 5. Sagittal plane head excursions for braced tests.

CONCLUSION

This study indicates that pre-impact bracing and sex influence occupant kinematics for volunteers during frontal sled tests that are similar to pre-crash braking events. Braced tests resulted in decreased peak forward excursions at all anatomical locations compared to relaxed tests for both sexes. In general, males displaced forward more than females when relaxed, but both sexes displaced forward similarly when braced. These sex differences, and their minimization during bracing, illustrate the importance of validating HBMs with appropriate volunteer data in order to accurately predict kinematics and injury risk for different demographics. Additionally, the observed decrease in forward displacements for both males and females during pre-impact bracing underscores the need to consider bracing scenarios in HBMs.

Changes in occupant kinematic response are especially important to consider when evaluating vehicle safety systems such as AEB. Specifically, altered occupant position due to pre-crash events may lead to differences in vehicle restraint effectiveness and potentially harmful interactions with the vehicle interior. This in turn can lead to altered injury risks and outcomes associated with frontal MVCs.

NOVELTY/TRAFFIC SAFEY IMPLICATIONS

As crash avoidance technologies become more prevalent in vehicles, occupant displacements due to pre-crash events become increasingly necessary to assess. Previous volunteer studies have evaluated occupant kinematics during pre-crash braking events, but few have included small female volunteers. This study quantified occupant kinematic response with a 1.1 g acceleration pulse, which is similar to a pre-crash braking event, and observed considerable occupant displacements as a result of the event for both small females and mid-sized males, even when bracing. Additionally, this study provides new female and male biomechanical response data that can be used to further develop and validate HBMs that incorporate active musculature, in order to better understand and assess injury risk in frontal MVCs.

ACKNOWLEDGEMENTS

The authors would like to thank the Global Human Body Models Consortium for funding this research and the volunteers who participated in this study.

REFERENCES

[1] Cicchino, J. B. Effectiveness of forward collision warning and autonomous emergency braking systems in reducing front-to-rear crash rates. Accid. Anal. Prev. 99 (A): 142-152, 2017.

[2] Reed, M. P., et al. Passenger head kinematics in abrupt braking and lane change events. Traffic Inj. Prev. 19 (sup2): S70-S77, 2018.

[3] Östh, J., et al. Muscle activation strategies in human body models for the development of integrated safety. ESV Conference Proceedings, 8-11, 2015.

[4] Ejima, S., et al. Prediction of the physical motion of the human body based on muscle activity during pre-impact braking. IRCOBI Conference Proceedings, 163-175, 2008.

[5] Östh, J., et al. Driver kinematic and muscle responses in braking events with standard and reversible pre-tensioned restraints: validation data for human models. Stapp Car Crash J. 13: 1-41, 2013.

[6] Beeman, S. M., et al. Effects of bracing on human kinematics in low-speed frontal sled tests. Ann. Biomed. Eng. 39 (12): 2998-3010, 2011.

[7] Carlsson, S. and Davidsson, J. Volunteer occupant kinematics during driver initiated and autonomous braking when driving in real traffic environments. IRCOBI Conference Proceedings, 125-136, 2011.

Sociodemographic variations in child restraint system use

Leah Lombardi, MPH
Drexel University Dornsife School of Public Health

Emma Sartin, PhD, MPH, Kristi Metzger, PhD, MPH, Melissa Pfeiffer, MPH, Meghan Carey, MS, & Allison Curry, PhD, MPH
Center for Injury Research and Prevention, Children's Hospital of Philadelphia

INTRODUCTION

Motor vehicle crashes are a leading cause of death in children: in 2017, 1,147 children under age 14 years died in motor vehicle crashes in the United States [1]. A critical component of reducing childhood injury and mortality risk in a crash is child restraint system (CRS) use. Unrestrained children are nearly three times more likely than restrained children to experience mortality and injury in a crash [2, 3]. Further, one study determined that 39% of fatally injured child passengers were unrestrained, revealing serious consequences for CRS non-use [4]. Though most children are restrained during vehicle trips, CRS non-use remains problematic [2]. There is evidence to suggest that there are differences in CRS use by child sex and age and specific driver characteristics.

Across all ethnic and age groups, males are more likely than females to die from all types of injury, and males make up 56% of child crash fatalities [5, 1]. An analysis of the Fatality Analysis Reporting System from 2008 through 2015 revealed that a larger proportion of males aged 0-2 years were unrestrained at the time of the crash than females aged 0-2 years [3].

With respect to age, children are to be restrained in a series of seats over time: they begin in a rear-facing CRS with a five-point harness, transition to a forward-facing CRS with a five-point harness, and finally move to a belt-positioning booster (BPB) seat [6]. Younger children—who are seated in rear- and forward-facing CRSs—are more likely to be restrained than older children [7]. A 2008 observational survey conducted by the National Highway Traffic Safety Administration found that 99% of children aged 12 months and younger were in a CRS but that restraint use decreased with age to 89% of 4- to 7-year-old children [7]. Four- to 7-year-olds are typically restrained in a forward-facing CRS or a BPB, but parents have reported that the cost of purchasing a BPB in addition to prior CRSs is a deterrent [8]. Overall, lower-income populations have decreased rates of CRS use [9]. However, research is limited, and many studies examining the impact of income on CRS use rely on self-report methods and small sample sizes.

Several other driver-level characteristics are also associated with CRS non-use, including not wearing a seatbelt, being male, alcohol or drug use, and being under 20 years old [3, 10]. These associations have mostly been identified in fatal crashes; we know less about CRS use among the general driver population.

Though CRSs are important for preventing childhood mortality in a crash, research has not fully elucidated the factors driving CRS non-use, particularly the interaction of child age and driver income. Thus, we analyzed data from a statewide data source in New Jersey—the New Jersey Safety and Health Outcomes (NJ-SHO) warehouse—to examine the association between CRS use and sociodemographic factors among children involved in police-reported crashes.

METHODS

The NJ-SHO warehouse contains linked data from several statewide data sources in New Jersey (NJ), including its crash database. This database includes data from all NJ police-reported crashes; crashes are reportable if they result in injury to a crash-involved person or property damage >$500 [11]. Crash data provides information about drivers and passengers, including restraint use (seatbelt and CRS), age, sex, and drug/alcohol use [11]. Each driver's residential address was geocoded and linked to publicly available census tract-level income data from the American Community Survey. In this study, NJ-SHO data was limited to include crashes from 2007 through 2014 involving child passengers under age 8 years old, as these children are required by NJ law to be in a CRS.

Variable Definitions

The outcome of interest was CRS use (yes/no). The child-level independent variables we examined were sex (male/female) and age (0-1, 2-3, and 4-7 years based on NJ's recommendations for transitioning between CRSs) [6]. The primary driver-level variable we examined was census tract-level median household

income quintile (Q1: <$46,099, Q2: $46,099-$63,468, Q3: $63,469-$80,567, Q4: $80,568-$103,020, and Q5: ≥$103,021). We also examined driver age (continuous, in years), sex (male/female), seatbelt use (yes/no), and suspected alcohol or drug use (yes/no).

Statistical Analysis

All statistical analyses were completed using SAS 9.4 (SAS Institute Inc., Cary, NC). We conducted a complete case analysis for participants lacking data for the variables of interest, followed by a log-binomial regression analysis. We used a nested analysis with an unstructured correlation structure to account for correlation among multiple children in the same vehicle, and we stratified into two adjusted models: one for male and one for female child passengers. These models contained the previously described independent variables and an interaction term between census tract-level median household income quintile and age**.**

RESULTS

This study included 159,251 children under age 8 years involved in motor vehicle crashes in NJ from 2007 through 2014. Males and females were equally represented in the study population: 50.6% vs. 49.4%, respectively. Within age categories, 18.2% of the study population was 0-1 years, 28.5% was 2-3 years, and 53.3% was 4-7 years. The proportion of females restrained in a CRS was similar to males (73.3% vs. 73.0%), indicating that there were no substantial sex-based differences in CRS use.

Adjusted for other variables, within the lowest income quintile, females aged 0-1 and 2-3 years were more likely to be restrained than females aged 4-7 years (Table 1). A similar pattern was seen for females in the highest income quintile but with a smaller magnitude of association, indicating that age-based differences may be more substantial among children in lower income quintiles (Table 1). These associations were also seen among male child passengers (Table 2).

Examining the impact of income, among both males and females, children in Q1 were less likely to be restrained than children in Q5 (Tables 1 & 2). This association was particularly pronounced among children aged 4-7 years; income-based differences were smaller among younger children (Tables 1 & 2). Similar patterns were seen for comparisons of other quintiles (Q2-Q4): children in lower income quintiles were less likely to be restrained than children of the same age in Q5, though with a smaller magnitude of association than Q1 vs. Q5, which was the focus of this study.

With respect to driver-level variables, although driver age and sex were not associated with CRS use, driver seatbelt use was associated with increased likelihood of CRS use (Tables 1 & 2). Suspected alcohol or drug use was associated with decreased likelihood of CRS use (Tables 1 & 2).

Table 1: Adjusted risk ratios and 95% confidence intervals for CRS use, females.

	RR	95% CI
Age within Income Quintiles		
0-1 vs. 4-7, Q1	1.80	1.75-1.86
2-3 vs. 4-7, Q1	1.64	1.59-1.70
0-1 vs. 4-7, Q5	1.25	1.23-1.27
2-3 vs. 4-7, Q5	1.24	1.22-1.26
Income within Age Groups		
Q1 vs. Q5, 0-1	0.92	0.90-0.94
Q1 vs. Q5, 2-3	0.85	0.83-0.86
Q1 vs. Q5, 4-7	0.64	0.62-0.66
Driver Sex		
Female vs. Male	1.06	1.05-1.07
Driver Age	1.00	1.00-1.00
Driver Seatbelt Use		
No vs. Yes	0.74	0.70-0.78
Suspected Alcohol or Drug Use		
Yes vs. No	0.90	0.85-0.97

Table 2: Adjusted risk ratios and 95% confidence intervals for CRS use, males.

	RR	95% CI
Age within Income Quintiles		
0-1 vs. 4-7, Q1	1.78	1.73-1.84
2-3 vs. 4-7, Q1	1.61	1.56-1.65
0-1 vs. 4-7, Q5	1.28	1.26-1.30
2-3 vs. 4-7, Q5	1.27	1.25-1.29
Income within Age Groups		
Q1 vs. Q5, 0-1	0.93	0.91-0.94
Q1 vs. Q5, 2-3	0.84	0.83-0.86
Q1 vs. Q5, 4-7	0.66	0.65-0.68
Driver Sex		
Female vs. Male	1.06	1.05-1.07
Driver Age	1.00	1.00-1.00
Driver Seatbelt Use		
No vs. Yes	0.76	0.72-0.81
Suspected Alcohol or Drug Use		
Yes vs. No	0.88	0.83-0.94

DISCUSSION

This study examined the association of various child- and driver-level variables with CRS use. In both sexes and across income quintiles, children aged 0-1 years and 2-3 years were more likely to be restrained in a CRS than 4- to 7-year-olds. In addition, using census tract-level median household income, disparities related to CRS use were identified; those in lower income quintiles were less likely to be restrained in a CRS than those in the highest income quintile. Age-based differences were more prominent in lower income quintiles compared with the highest income quintile. The size of association was similar for males and females, indicating that the impact of age and income may not differ by sex. At the driver level, not wearing a seatbelt and suspected drug or alcohol intoxication were associated with decreased CRS use. The findings from this study make it clear that targeting CRS availability and use in lower income neighborhoods is an important area of intervention to improve child safety outcomes.

CONCLUSION

Age and census tract-level median household income impact a child's likelihood of being restrained in a CRS. Findings from this study are consistent with previous research that suggests that children who are older and of lower socioeconomic status are less likely to be restrained. Critically, this study revealed that although older children were less likely to be restrained than younger children across income quintiles, there were particularly large differences by age for those in the lowest-income census tracts. This finding has important policy implications, such as making CRSs—particularly BPBs—more affordable or available for children in low-income neighborhoods.

These differences were observed among both males and females, despite the fact that males are at greater risk of injury and death in a crash. Research should continue to explore the factors at play in males' increased risk.

NOVELTY/TRAFFIC SAFEY IMPLICATIONS

The NJ-SHO is a source of objective data for this topic area that does not rely solely on fatal crash data or survey reports. The NJ-SHO incorporates all police-reported crashes occurring over an 8-year time period in NJ; its large sample size allows for an examination of multiple factors with reasonable confidence in the estimates. By examining the interaction of age and census tract-level income, this study highlighted a particular group that may be at risk for not using a CRS, and thus increased risk of fatality in a crash: low-income 4- to 7-year-old children.

ACKNOWLEDGEMENTS

The author thanks Félice Lê-Scherban, PhD, MPH at the Drexel University Dornsife School of Public Health for her assistance on this project. She did not receive compensation for her contributions. The author also thanks the New Jersey Department of Transportation and the New Jersey Motor Vehicle Commission for providing data.

REFERENCES

[1] National Center for Statistics and Analysis, "Children: 2017 Data," Retrieved from https://crashstats.nhtsa.dot.gov/Api/Public/ViewPublication/812719, 2019.
[2] Decina, L. E., & Lococo, K. H., "Child restraint system use and misuse in six states," *Accident Analysis and Prevention*, vol. 37, no. 3, pp. 583–590, 2005.
[3] Huang, Y.-Y., Liu, C., & Pressley, J. C., "Restraint use and injury in forward and rear-facing infants and toddlers involved in a fatal motor vehicle crash on a U. S. Roadway," *Injury Epidemiology*, vol. 6, no. S1, pp. 1–11, 2019.
[4] Sherwood, C. P., Ferguson, S. A., & Crandall, J. R., "Factors leading to crash fatalities to children in child restraints," *Association for the Advancement of Automotive Medicine*, vol. 47, pp. 343–359, 2003.
[5] Sorenson, S. B., "Gender disparities in injury mortality: Consistent, persistent, and larger than you'd think," *American Journal of Public Health*, vol. *101*(SUPPL. 1), pp. 353–358, 2011.
[6] Lampitt, P. R., Beach, J., & Allen, D., "Assembly, No . 3083 State of New Jersey 216th Legislature," 2014.
[7] NHTSA, "Child Restraint Use in 2008—Overall Results," Retrieved from https://crashstats.nhtsa.dot.gov/Api/Public/ViewPublication/811135, 2009.
[8] Simpson, E.M., Moll, E.K., Kassam-Adams, N., Miller, G.J., Winston, F.K., "Barriers to Booster Seat Use and Strategies to Increase Their Use," *Pediatrics*, vol. 110, no. 4, pp. 729-736, 2002.
[9] Brixey, S., Ravindran, K., & Guse, C.E., "Legislating child restraint usage- Its effect on self-reported child restraint use rates in a central city," *Journal of Safety Research*, vol. 41, no. 1, pp. 47-52, 2010.
[10] Privette, F., Nwosu, A., Pope, C., Yang, J., Pressley, J., & Zhu, M., "Factors Associated with Child Restraint Use in Fatal Motor Vehicle Crashes." *Clin Pediatr (Phila)*, vol. 57, no. 12, pp. 1423–1431, 2018.
[11] State of New Jersey Motor Vehicle Commission, "NEW JERSEY NJTR-1 Crash Report Manual," Retrieved from http://www.state.nj.us/transportation/refdata/accident/pdf/NJTR1-Guidebook.pdf, 2017.

Examination of Restraint Sensitivity and Validation of the PIPER 6-Year-Old Model

Matthew Miller
Center for Applied Biomechanics, University of Virginia

Daniel Perez-Rapela, Bronislaw Gepner, Jason Forman
Center for Applied Biomechanics, University of Virginia

INTRODUCTION

Automotive crashes are the leading cause of death for children in the United States aged one to seventeen years [1]. Children are a vulnerable population in motor vehicle crashes as standard restraints are positioned to engage the adult upper body. Belt-positioning booster seats aid in the transition as a child outgrows a dedicated child seat (with a multi-point harness), but is not yet tall enough to properly engage with a vehicle seat and seatbelt. Booster seats raise the child above the seatpan and reroute the lap belt, with the goal of improving occupant restraint engagement.

Finite element human body models (HBMs) can provide data on child response in crashes. The PIPER HBM is a scalable child model representing a 6-year-old in its stock configuration [2]. The HBM validation consisted of physical tests using post-mortem human subjects, anthropomorphic test devices, and volunteers. These simulations are provided with PIPER in a prepackaged validation suite.

The objective of this work is to gain an understanding of the PIPER model's sensitivity to various restraint conditions, including belt anchorage locations and presence of a booster seat. Particular areas of interest include head excursion and submarining. Submarining occurs when the occupant slides below the lap belt during a collision, causing the belt to load the abdomen rather than the pelvis. The biofidelity of PIPER was also examined using the provided validation suite in support of this goal.

METHODS

The validation of the HBM was examined by selecting nine of the provided validation cases that were highly relevant to this study. These validation cases included belt pull, impact, and sled tests. Simulations were conducted in LS-DYNA v.9.1.0 using the publicly available PIPER HBM. The in-house results were compared to those provided by PIPER's developers and data from the original studies. The model performance was graded on a four-tier scale of good, acceptable, marginal, and poor. In addition, several of the validation cases were modified to examine PIPER's stability in extreme conditions. Specifically, for selected sled test cases the severity of the acceleration pulse was increased and the restraints were modified to check the stability of the model under high-severity loading conditions.

For the submarining sensitivity study, four different anchorage scenarios were selected (Figure 1) based on the Insurance Institute for Highway Safety (IIHS) Booster Seat Testing Protocol [3]. These scenarios are based on two lap belt anchorage locations (forward/aft) and two shoulder belt anchorage locations (low, outboard/high, inboard). These layouts represent the range of anchorage locations observed in the field. Each of the scenarios were tested with and without a representative booster seat provided in the PIPER HBM download, and with three different child seating postures. The seating postures were selected to represent different degrees of occupant slouch based on recently published child posture data [4]. The slouch postures were achieved by translating the pelvis 25 mm and 50 mm forward from its upright posture before settling the occupant. The occupant was later settled by gravity and the resulting stress state was transferred to the final simulation. The seatbelt was positioned using an in-house MATLAB automation that ensures that the webbing follows the shortest path. The resulting 24 simulations were subjected to the FMVSS 213 acceleration pulse. Submarining was defined as the lower edge of the lap belt moving posterior relative to the anterior superior iliac spine (ASIS).

RESULTS

44% of the relevant validation cases were evaluated as good, 22% acceptable, 33% marginal, and 0% poor. Scoring the results on a 0-3 scale (0 being "poor", 3 being "good") the average was 2.1. The model was shown to be stable in extreme cases, as the modified high-severity simulations were successful.

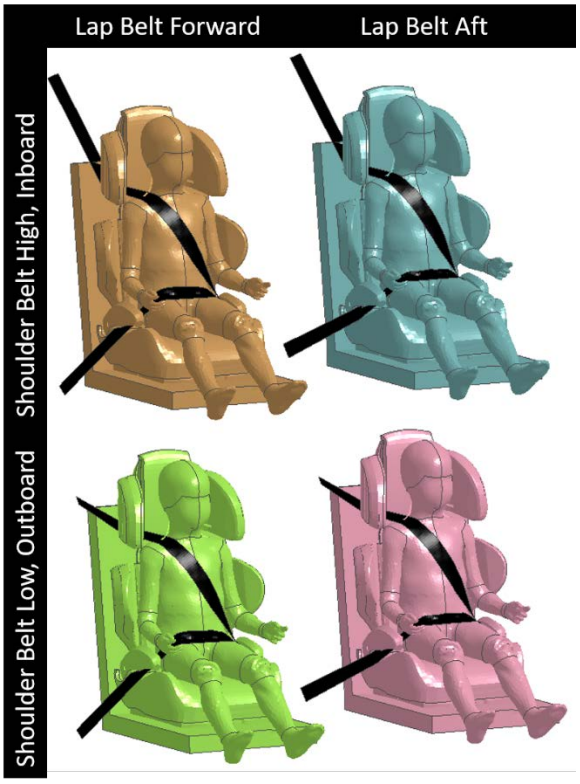

Figure 1. Seatbelt anchorage scenarios with representative booster

The model did not exhibit submarining in any of the upright-posture simulations regardless of the seatbelt configuration and the presence of a booster, though the booster did affect the trajectory of the belt relative to the pelvis. The model submarined in two of the non-booster moderate slouch posture simulations, and two of the non-booster extreme slouch postures. In addition, one of the booster simulations exhibited occupant submarining in the extreme slouch posture (Table 1). Lap belt anchors were in the aft position for all cases that submarined (Figure 3).

Head excursion in the fore/aft direction ranged from a minimum of 294 mm to a maximum of 437 mm across all simulations. Simulations without boosters had a slightly lower head excursion than the comparable booster simulations. In addition, simulations with the low/outboard shoulder belt anchor had a larger head excursion than those with the high/inboard anchor position.

The booster played an important role in routing the seatbelt webbing. The cases without booster presented suboptimal shoulder belt placement including cases where the shoulder belt was directly in contact with the HBM's neck (Figure 2). These deficiencies in shoulder belt engagement translated into increased contact forces with the neck region.

Table 1. Simulation matrix and submarining results

	Posture	Lap Belt Anchors	Shoulder Belt Anchors	Result
No Booster	Upright	Forward	Low, Outboard	No Submarining
			High, Inboard	No Submarining
		Aft	Low, Outboard	No Submarining
			High, Inboard	No Submarining
	Moderate Slouch	Forward	Low, Outboard	No Submarining
			High, Inboard	No Submarining
		Aft	Low, Outboard	Submarining
			High, Inboard	Submarining
	Extreme Slouch	Forward	Low, Outboard	No Submarining
			High, Inboard	No Submarining
		Aft	Low, Outboard	Submarining
			High, Inboard	Submarining
Booster	Upright	Forward	Low, Outboard	No Submarining
			High, Inboard	No Submarining
		Aft	Low, Outboard	No Submarining
			High, Inboard	No Submarining
	Moderate Slouch	Forward	Low, Outboard	No Submarining
			High, Inboard	No Submarining
		Aft	Low, Outboard	No Submarining
			High, Inboard	No Submarining
	Extreme Slouch	Forward	Low, Outboard	No Submarining
			High, Inboard	No Submarining
		Aft	Low, Outboard	Submarining
			High, Inboard	No Submarining

Figure 2. Example of poor seatbelt fit in an upright posture without booster

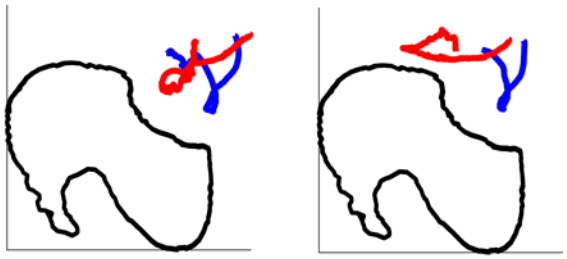

Figure 3. Motion of the lapbelt lower edge wrt. the pelvis for moderate-slouch cases with (blue) and without (red) booster. All traces correspond to simulations with high shoulder belt anchorage, and fore (left) and aft (right) lap belt anchorage.

DISCUSSION

The preliminary results of this study generally follow expected submarining patterns. Moving the occupant's pelvis forward (increasing slouch and increasing pelvis angle) increases the likelihood and severity of submarining. The introduction of the booster improves seatbelt routing and decreases the likelihood of submarining. The PIPER model also shows sensitivity to lap belt anchorage location. All four non-booster slouched simulations with aft lap belt anchorage resulted in submarining, while none of the forward lap belt anchorage simulations submarined. The aft anchorage locations create a more horizontal force vector, encouraging rotation of the pelvis and movement of the belt above the ASIS. In contrast, the forward lap belt anchors create a more downward force vector, keeping the belt from sliding up over the ASIS.

CONCLUSION

Preliminary results show the occurrence of submarining with this model to be sensitive to belt anchorage location and presence of a booster seat, suggesting a potential utility in evaluating restraint or booster geometry (though there is presently not sufficient reference data to evaluate the validity of this sensitivity). The results of the validation suite correspond well with the data from the underlying studies. PIPER performs particularly well in tests where kinematics is a primary concern, such as head excursion in whole-body tests. In addition, the model's stability in high-severity conditions encourages use over a wide range of input conditions other than the standard FMVSS 213 pulse.

NOVELTY/TRAFFIC SAFEY IMPLICATIONS

The PIPER HBM is a tool with high utility for simulating child response in motor vehicle crashes. The PIPER model's submarining is sensitive to anchorage position, seating posture, and the presence of a booster seat. A scalable HBM such as PIPER will be invaluable for both restraint design and analysis. This preliminary work to examine PIPER's restraint sensitivity, validation, and stability is one step towards building confidence in the model for widespread use.

ACKNOWLEDGEMENTS

This study is supported by the Insurance Institute for Highway Safety.

REFERENCES

[1] Truong WH; Hill BW; Cole PA; (2013) Automobile Safety in Children: a Review of North American Evidence and Recommendations. *Journal of the American Academy of Orthopaedic Surgeons*, 21(6): 323-331.

[2] Beillas, P.; Giordano, C.; Alvarez, V.; Li, X.; Ying, X.;et al.. Development and performance of the PIPER scalable child human body models. *14th International Conference on the Protection of Children in Cars*, Dec 2016, MUNICH, Germany.

[3] Insurance Institute for Highway Safety. Booster Seat Belt Fit Evaluation Protocol (Version IV) Insurance Institute for Highway Safety; Ruckersville, VA, USA. Available online: http://www.iihs.org/iihs/ratings/technical-information/boosterprotocols.

[4] Jones, M.L.; Ebert, S.; Manary, M.A.; Reed, M.P.; Klinich, K.D. Child Posture and Belt Fit in a Range of Booster Configurations. *Int. J. Environ. Res. Public Health* 2020, 17, 810.

Emergency Response to Vehicle Collisions: Feedback from Emergency Medical Service Providers

Jacob T. Valente
Virginia Tech Biomedical Engineering and Mechanics Department; Virginia Tech Transportation Institute

Miguel A. Perez
Virginia Tech Biomedical Engineering and Mechanics Department; Virginia Tech Transportation Institute

INTRODUCTION

Though the safety of vehicles has increased with the incorporation of advanced crash avoidance and mitigation features, the National Highway Traffic Safety Association reported 37,133 fatal crashes in 2017, representing only a 2% decrease in the number of fatal crashes compared to 2016 [1]. When motor vehicle crashes occur, victims rely on emergency medical services (EMS) to provide them with care. A number of factors can affect the quality and efficiency of these services. Consequently, in efforts to improve emergency response to motor vehicle collisions (MVCs), previous research has developed injury risk predictions based on vehicle kinematics [2] and suggested options for improved dispatching of EMS to MVCs [3]. Collectively, these and many other studies highlight the need for real-time, accurate, and increased MVC data. While the benefits obtained from such data are understood, the actual data components that would be most useful and relevant are still unclear. Hence, this study interviewed emergency medical technicians (EMTs) to collect feedback on their experiences as a means to better understand the challenges faced by EMS providers when responding to MVCs and to identify specific information elements that would improve their ability to respond to MVCs and perform effective and efficient crash victim care.

METHODS

This study was conducted by interviewing 15 EMTs from southwest Virginia and was approved by the Virginia Tech Institutional Review Board. The interviews consisted of 10 questions; the first five questions requested feedback surrounding difficulties faced during initial MVC response; questions six and seven requested desired information that would lead to improved response or care; and questions eight through ten collected information on EMT-observed trends and the feedback process between themselves and medical treatment facilities. The interviewed EMTs practiced in six different locations within southwest Virginia and operated in a mix of rural, suburban, and urban communities.

All interviews were documented through handwritten notes, and audio was recorded when consented. The notes were then transcribed. Answers to the questions were separated into unique thoughts to accommodate the varied participant experience and responses. A unique thought was identified as an independent topic that was often preceded and followed by pauses or obvious verbal confirmation. Each unique participant thought was separated by theme, modeled on the study done by Terry, et al. (2018) [4]. The list of themes was developed by generalizing commonalities between interview responses. To avoid themes that were either too vague or too specific, the themes were iterated several times as new content was analyzed. An “other” category was used to capture unique thoughts that could not be classified cleanly in other themes.

RESULTS

The first five questions targeted feedback on the challenges faced during dispatching, initial response, and travel surrounding MVCs. The frequency of occurrence for the themes extracted from the collected responses is listed in Figure 1. The most common theme highlighted concerns around the lack and inaccuracy of the MVC information provided to EMTs. The second most frequent theme represented the various difficulties that EMTs encounter when interacting with traffic, including but not limited to, delays in response time and unpredictable drivers/driver behavior. The third most mentioned theme was the mismatch in communication technology used by medical facilities, cooperating EMS entities, and local infrastructure. Additional themes included scene safety, resource allocation and management, and timely notification of MVC and/or MVC severity. The “other” category included thoughts related to helicopter accessibility, hospital interactions, and training.

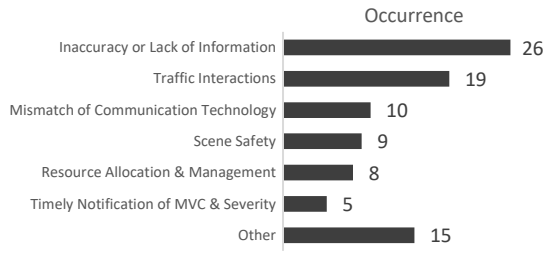

Figure 1.Themes that described difficulties faced by EMTs that arise during dispatching and travel when responding to MVCs.

The responses to questions six and seven were thematically grouped to elaborate on the information that most EMTs thought would improve the efficiency and quality of their MVC response and patient care. The themes were first separated by information source: the vehicle, the occupant, or the roadway. This totaled six vehicle-based themes, three occupant-based themes, and three roadway based-themes (Figure 2). Of the vehicle-based themes, the most prominent was data elements, such as GPS location, propulsion mechanism, and airbag location. Next was deformation and extraction, which aimed at gaining better information to estimate the possibility of entrapment and damage to the cabin. The remaining vehicle-based themes included kinematics, hazard detection, and rollover detection. The "other" category contained comments on automatic hazard light activation, the number of vehicles involved, and easy on-scene retrieval of the requested data.

Within the occupant-based data category, the most common theme was occupant details and passive safety interactions. This indicated EMTs' desire to have information about the number of occupants, their location, who was belted, and who interacted with airbags. The second theme was vitals, which included measurements such as heart rate, pulse, respiratory rate, and consciousness. The "Other" category for occupants mostly included comments on preregistration of health conditions.

EMTs indicated, within the roadway theme, benefitting from quicker and more accurate traffic updates and programable signs. There were also calls for roadway design improvements that catered towards improved emergency response (e.g., wider shoulders, emergency lanes that do not alternate sides of the roadway). The "other" category in this theme included concerns for helicopter access and identification/signage of alternate routes compliant with emergency vehicle requirements.

In the question about observed trends in MVCs, a majority of the participants indicated that they have observed a correlation between crash types and injury characteristics, but the relationships mentioned were predominantly well-known injury mechanisms. Feedback loops between EMTs and medical facilities appeared to be existent: all participants claimed to receive feedback on their performance from hospital staff upon request and noted that this feedback is typically used in subsequent training. Additional comments mainly emphasized previously discussed topics.

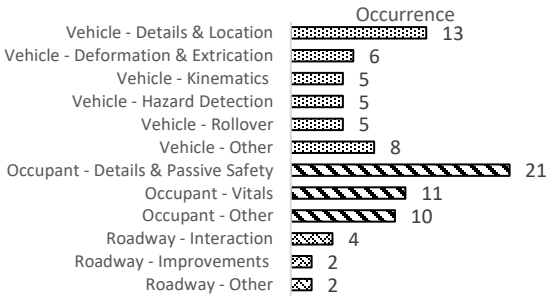

Figure 2. Themes that represent desired information to improve EMT effectiveness and efficiency when responding to MVCs.

DISCUSSION

Information inaccuracies, timely notification of crashes, and resource allocation were expected to be common topics during the interviews. All three of these themes were indeed thoroughly discussed and, as elaborated by the participants, found to influence each other greatly. The information received for a particular MVC can be extremely variable depending on the individual reporting it and their training. Further, in conditions where vehicle occupants may be incapacitated, do not have cellular service, or when the vehicle is no longer visible to potential bystanders, obtaining a timely, accurate, and detailed notification of an MVC is critical for the victims' safety. A faster and accurate notification directly leads to faster responses and deployment of appropriate resources. This can include extrication tools or enough supplies and personnel to treat all victims, which improves the quality of care. In terms of scene safety, participants indicated that EMS personnel greatly rely on truck positioning for protection, often not being able to begin care until another vehicle is present to reduce risk. Even then, only limited additional safety may be gained by the presence of a blocking vehicle.

Some unanticipated themes also emerged throughout the interviews. Considering modern advancements in radio and cellular devices, the mismatch between dispatching and communication technology was a surprising but frequently mentioned difficulty. Gaps in

communication due to incompatible devices are compounded by limits within those communication tools in terms of the quantity and quality of the information that can be communicated. These limits force dispatchers or EMS to be selective about what and when information is shared. Another unanticipated theme concerned the difficulties that accompany traffic interactions. This issue is relevant not only when traveling to an MVC but also when traveling to a medical center. Maneuvering through dense traffic and dealing with unpredictable (and sometimes unwilling) drivers not only greatly increases response time but can increase the likelihood of another safety critical event occurring.

Interview questions related to information needs revealed that most of the desired information is related to the vehicle and its occupants. It was expected that kinematic data and rollover detection would be requested to assist in injury prediction, and these were indeed identified by interviewees. However, interviewees also expressed interest in information about vehicle deformation, particularly of the cabin. Many participants voiced how helpful these measurements may be to anticipate entrapment and deploy the necessary tools during the initial response. Requests for vehicle make, model, and a more precise event location were also common, along with a call for early detection of potential hazards. Specifically, potential hazards mentioned included vehicle propulsion systems, non-deployed airbag locations, commercial vehicle cargo, and presence of fire or water.

As expected, occupant-based data needs included measurements of occupants' vitals as a way to help predict trauma. Pre-existing conditions, and the ability to register these with a vehicle, were also mentioned as potentially beneficial for older or compromised driving populations susceptible to sudden onset medical emergencies. The call for basic occupant details like location in the vehicle and seatbelt usage was greatly emphasized. This information would help shape the initial EMT response to ensure that an appropriate number of supplies is available to treat all victims and to allow EMS to better prepare their triage strategy before arrival.

CONCLUSION

Collectively, the compiled themes and the corresponding comments from EMTs clarify and put in context some areas for improvement in emergency response to MVCs. In general, information about MVCs needs to encompass specific areas, be more accurate, and be communicated faster. This would allow better EMS resource allocation and EMT personnel management. These goals can be further enabled by providing more detailed vehicle-based information (e.g., precise location, deformation approximations, or vehicle hazards) and occupant-based information (e.g., vital measurements and occupant interactions with safety systems). These requirements may be considered in the development and design of advanced automotive collision notification systems, which are becoming more prevalent in the vehicle fleet.

NOVELTY AND TRAFFIC SAFETY IMPLICATIONS

In general, the results point to some novel areas of improvement in communicating and responding to MVCs. As expressed by the interviewees, traffic interactions between EMS and the public need to be improved in order to reduce response times and increase public safety. In addition, better resource allocation and compatible communication technology will assist in attaining faster EMS response times and in optimizing system response when multiple MVCs occur in close temporal and spatial proximity. Better understanding of potential hazards before on-scene arrival will increase the safety of both victims and responding EMS. Better understanding of victim conditions may also lead to more appropriate treatment that could decrease the likelihood of severe injury or fatality. Finally, immediate transmission of relevant data to EMS would assist with improving the rapidity and quality of EMS response to MVCs.

REFERENCES

[1] National Center for Statistical and Analysis. (2019, August) *State traffic data: 2017 data* (Traffic Safety facts. Report No. DOT HS 812 780). Washington, DC: National Highway Traffic Safety Administration

[2] Weaver, A. A., Talton, J. W., Barnard, R. T., Schoell, S. L., Swett, K. R., & Stitzel, J. D. (2015). Estimated Injury Risk for Specific Injuries and Body Regions in Frontal Motor Vehicle Crashes. *Traffic Injury Prevention*, *16*(sup1).

[3] Amorim, M., Ferreira, S., & Couto, A. (2018). Emergency Medical Service Response: Analyzing Vehicle Dispatching Rules. *Transportation Research Record: Journal of the Transportation Research Board*, *2672*(32), 10–21.

[4] Terry, T., Trimble, T. E., Blanco, M., Fitzgerald, K. E., Fitchett, V. L., and Chaka, M. (2018). *An Examination of Emergency Response Scenarios for ADS*. Farmington Hills, MI: Crash Avoidance Metrics Partners LLC.

Development and Validation of an Active Small Female and Average Male Human Body Model for Predicting Head Kinematics in Pre-Crash Braking and Low-Speed Frontal Sled Tests

Karan S. Devane
Center for Injury Biomechanics, Virginia Tech–Wake Forest University

Hana Chan, Devon L. Albert, Andrew Kemper, F. Scott Gayzik
Center for Injury Biomechanics, Virginia Tech–Wake Forest University

INTRODUCTION

Recent literature suggests that a vehicle occupant's active muscle response is a significant factor in predicting posture following pre-crash maneuvering or braking [1, 2]. Active human body models (AHBM) are necessary to predict occupant posture during pre-crash as well as low-speed impacts. The effect of occupant bracing is prominent in these cases. The differences in occupant kinematics between male and female volunteers [1, 2] have motivated researchers to develop AHBMs of different sizes and sexes. The objective of this study was three-fold; to develop a computationally-efficient small female (54.1 kg, 149.9 cm) finite element model with active muscles, to check the suitability of this model along with an average male (78.4 kg, 174.9 cm) active model for predicting head kinematics during pre-crash braking and low-speed frontal sled tests, and finally to validate the predicted head kinematics against volunteer experiments with subjects representing 5th percentile female and 50th percentile male.

METHODS

The Global Human Body Models Consortium (GHBMC) 50th percentile male simplified occupant model with active musculature (M50-OS+Active v2.2) [3] was used in this study. The model for representing female subjects was developed by adding active elements representing skeletal muscles (n = 232) to the GHBMC 5th percentile female simplified occupant model (F05-OS v2.2) to generate the F05-OS+Active model. The active muscle modeling strategy, muscle properties, and physiological cross-sectional area (PCSA) for each muscle were taken from the M50-OS+Active model [3]. The PCSAs were mass scaled to a 5th percentile female. The reaction delay, neural excitation delay, and muscle activation/deactivation delays were implemented in both of these models using a first-order low-pass filter calculated using Equation 1. The values for the delays were taken from various literature sources [4, 5]. The active models employ a PID controller based muscle activation strategy.

$$x(t_n) = x(t_{n-1}) + (input - x(t_{n-1})).\frac{dt}{(T + dt)}$$

Equation 1: First-Order Low-Pass Filter, T-time delay constant, t-time, dt-timestep, x-filtered signal

A total of 16 simulations were carried out. These simulations utilized two muscle conditions (relaxed and braced), two acceleration pulses (1.1g and 2.5g), two versions of the female model (F05-OS, i.e., control and F05-OS+Active), and two versions of the male model (M50-OS, i.e., control and M50-OS+Active). The control models have no muscle activation. The models were gravity settled in the seat, belted, and positioned in a driving posture similar to the initial posture of volunteers in experiments before simulations were run, as shown in Figure 1. The control model was run in matched simulations for the relaxed and braced conditions, without muscle activation. A 1.1g pre-crash braking pulse and a 2.5g low-speed pulse was used in these simulations. Head kinematics from the model were compared with the experimental data.

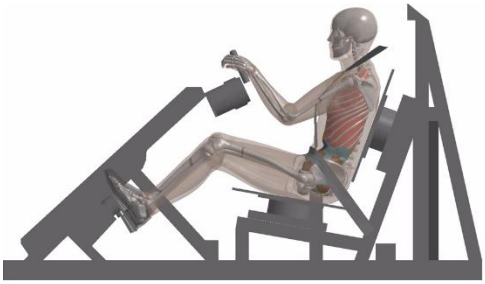

Figure 1: Simulation Setup for F05-OS+Active

Data Sources

Kinematics of three female and male volunteers, representing approximately 5th percentile and 50th percentile body habitus, respectively, were measured during pre-crash braking and low-speed frontal sled tests performed using a rigid test buck. All procedures were reviewed and approved by the Virginia Tech IRB. Each volunteer was subjected to two acceleration pulses with two muscle conditions (relaxed and braced). Head kinematics were measured using a VICON motion capture system and a 6-DOF accelerometer package placed on a mouthpiece. Head CG forward excursions were used for comparing simulation results. The sled buck was modeled using CAD data.

RESULTS

The head CG forward excursion results of both active models are shown in Figure 2-Figure 5. Each head CG displacement plot contains experimental data for three volunteers and two models (active and control) in both relaxed and braced muscle conditions. Active and control simulations showed clear differences. For both sexes in the pre-crash braking pulse, both active and control models for the relaxed state showed a concave down trajectory with the active model's forward excursion exceeding the control model's. In contrast, in the low-speed crash pulse, the active model's response was lower than the control model. However, for the braced simulation, the control model remained in the concave down trajectory while the braced model was more linearly downward, as the volunteers. This trend was observed throughout all simulations.

DISCUSSION

The downward trajectory of the volunteers, which is a function of muscle bracing, is captured in the active models but not in the control models. In the relaxed muscle condition, there was no significant difference between control and active model results. The head CG forward excursion for 1.1g is greater than 2.5g in the experimental as well as simulation results.

The head CG forward excursion in both muscle condition for males was greater than female volunteers, and the same observations were made with simulation results. This suggests the need for two different models for occupant kinematics prediction, although it is unclear if the results are a function of seated height alone at this time.

The updated neural delay method was supported by literature sources [4, 6] and was physiologically accurate compared to the previous implementation using a simple time shift [3].

Pre-crash braking events are of longer duration, and to simulate these events, the active model should be computationally efficient. The simplified models used in this study are 30-50 fold more computationally efficient than their detailed GHBMC model counterparts [7]. This makes these models suitable for replicating pre-crash scenarios.

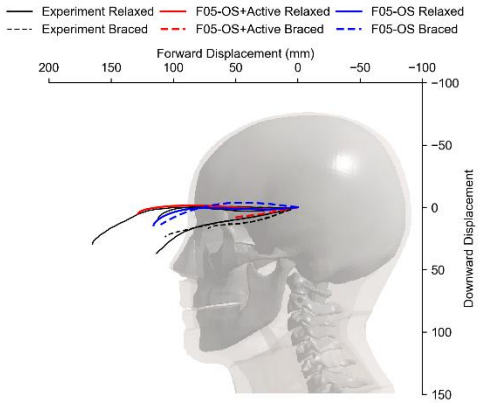

Figure 2: Head CG Forward Excursion in 1.1g Pre-Crash Braking Pulse for Female, solid line - relaxed muscle condition, dashed line – braced muscle condition

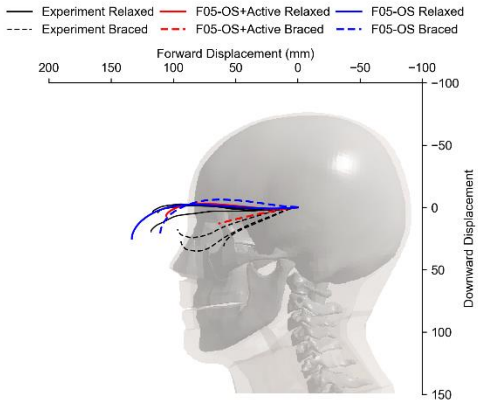

Figure 3: Head CG Forward Excursion in 2.5g Low-Speed Crash Pulse for Female, solid line - relaxed muscle condition, dashed line – braced muscle condition

CONCLUSION

The preliminary data presented in this study indicate that the selected modeling approach is capable of capturing the altered volunteer kinematics observed in the braced condition and reasonably captures relaxed condition response. This is an essential attribute of active models focused on the effects of vehicle dynamics on occupant posture.

NOVELTY/TRAFFIC SAFETY IMPLICATIONS

This study presents the validation of a female and male active finite element models using the size and sex-specific volunteer data. To the author's knowledge, this study is the first to use ad-hoc female-specific volunteer data in pre-crash braking and low-speed impact. A computationally efficient model is imperative in this application, given the duration of the events simulated, in all cases higher than 500 ms. Active HBMs are a valuable tool for engineers to explore the effects vehicle maneuvers have on occupants.

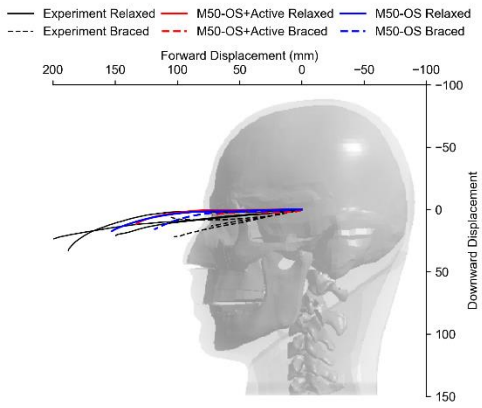

Figure 4: Head CG Forward Excursion in 1.1g Pre-Crash Braking Pulse for Male, solid line - relaxed muscle condition, dashed line – braced muscle condition

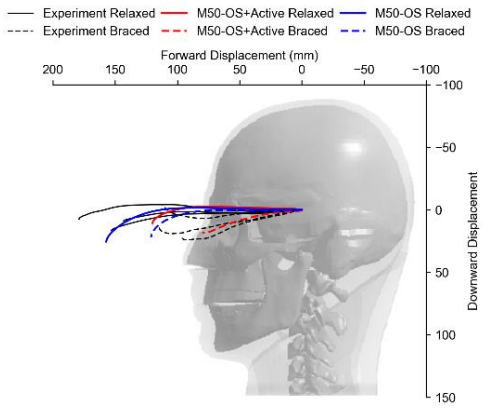

Figure 5: Head CG Forward Excursion in 2.5g Low-Speed Crash Pulse for Male, solid line - relaxed muscle condition, dashed line – braced muscle condition

ACKNOWLEDGEMENTS

All simulations were run on the DEAC cluster at Wake Forest University with support from Stevens Cody and Adam Carlson. The Global Human Body Models Consortium supported this study under contract WFU-006.

REFERENCES

[1] J. Osth, J. M. Olafsdottir, J. Davidsson, and K. Brolin, "Driver kinematic and muscle responses in braking events with standard and reversible pre-tensioned restraints: validation data for human models," *Stapp Car Crash J*, vol. 57, pp. 1-41, Nov 2013. [Online]. Available: https://www.ncbi.nlm.nih.gov/pubmed/24435725

[2] J. M. Olafsdottir, J. Östh, J. Davidsson, and K. Brolin, "Passenger kinematics and muscle responses in autonomous braking events with standard and reversible pre-tensioned restraints," in *International Research Council on Biomechanics of Injury*, Gothenburg, Sweden, 2013, no. IRC-13-70, pp. 602-617.

[3] K. Devane, D. Johnson, and F. S. Gayzik, "Validation of a simplified human body model in relaxed and braced conditions in low-speed frontal sled tests," *Traffic Injury Prevention*, vol. 20, no. 8, pp. 832-837, 2019/11/17 2019, doi: 10.1080/15389588.2019.1655733.

[4] J. Osth, K. Brolin, and R. Happee, "Active muscle response using feedback control of a finite element human arm model," *Comput Methods Biomech Biomed Engin*, vol. 15, no. 4, pp. 347-61, 2012, doi: 10.1080/10255842.2010.535523.

[5] J. Osth, K. Brolin, S. Carlsson, J. Wismans, and J. Davidsson, "The occupant response to autonomous braking: a modeling approach that accounts for active musculature," *Traffic Inj Prev*, vol. 13, no. 3, pp. 265-77, 2012, doi: 10.1080/15389588.2011.649437.

[6] R. Meijer, E. Van Hassel, J. Broos, H. Elrofai, L. Van Rooij, and P. Van Hooijdonk, "Development of a multi-body human model that predicts active and passive human behaviour," in *Proceedings of the International Conference on Biomechanics of Impact IRCOBI, Dublin-Ireland*, 2012, pp. 622-636.

[7] D. Schwartz, B. Guleyupoglu, B. Koya, J. D. Stitzel, and F. S. Gayzik, "Development of a computationally efficient full human body finite element model," *Traffic injury prevention*, vol. 16, no. sup1, pp. S49-S56, 2015.

Method to Capture Naturalistic Pedestrian Behavior in Virginia Traffic Camera Data

Max Bareiss, Hampton C. Gabler
Virginia Tech

INTRODUCTION

Future automated vehicle systems will need an understanding of pedestrian behavior to perform normal driving and prevent collisions. Traditionally, information on pedestrian behavior has come from observational studies in which pedestrians were observed at a fixed number of locations for a fixed period of time. Bosina and Weidmann [1] present a detailed review of pedestrian observational studies. In these studies, however, no consideration was made for pedestrians who were not crossing at a crosswalk. Mid-block crossings are a common occurrence: over two-thirds (68%) of pedestrian fatalities in the United States each year do not occur at an intersection [2].

Previous observational studies [1], [3] have relied on positioning cameras or observers near pedestrian crossing locations and observing behavior. Because the researchers in these studies position the cameras themselves, the selection of data collection sites can be driven by convenience. In this work we propose to overcome this limitation by observing pedestrian behavior using pre-existing traffic cameras in the Commonwealth of Virginia. These traffic cameras are located across the commonwealth and no physical setup is required for their use. This allows the locations to be easily selected and changed as part of the sample design.

The objective of this work was to develop a new method to study pedestrian behavior using traffic camera video. The promise of this new technique will be demonstrated by analyzing differences between mid-block pedestrian crossings and crosswalk crossings.

METHODS

Video Dataset

The source of video in this work was the Virginia Traffic Information system [4]. A total of 1,263 cameras were available at the time of this study. The underlying codec for all video streams was H.264. Not all video streams had the same frame rate, resolution, and bit rate, but most were approximately 15 frames per second, 320x240 (QVGA) resolution, and 200 kb/s. An example frame is shown in Figure 1.

Figure 1. An image from the camera located at the intersection of Kings Highway and Richmond Highway in Alexandria, Virginia. This image was captured at approximately 2:44:34PM on March 22, 2020. A pedestrian is visible crossing the center concrete divider on Richmond Highway, highlighted in the orange circle.

This work used a subset of cameras from a larger dataset. Five cameras were selected by manually reviewing video streams. Cameras were selected where a mid-block pedestrian crossing was visible in a separate data sample collected on March 22, 2020 between 2:00PM an 2:59PM. In the larger dataset, video from all Virginia cameras was recorded, starting at 4:00PM on December 17, 2019. Recording all Virginia camera streams was a considerable technical challenge.

Traffic camera video capture was accomplished using a custom application written in C++. Video stream processing was performed using the FFmpeg suite of open source libraries [5]. The capture application ran on six virtual machines located within the Virginia Tech Advanced Research computing (VT ARC) on-campus cloud. Data was stored using the VT ARC working file system for temporary access, and on their tape-based archive for long-term backup. Total data production was approximately 2.2TB per day.

Video Processing

The first step of video processing was to detect pedestrians. Pedestrians were detected using the open source human pose estimation library OpenPifPaf [6] in each frame of video. The detection process was performed on one node of the Huckleberry supercomputer [7] using all four NVIDIA P100 GPUs available. A total of 1,965 hours of video were processed at a rate 37 times faster than real-time. For each person visible in each frame, the output of the detection process was the location of the 17 joint locations annotated as part of the COCO Keypoint Detection Task [8] and the model confidence in those detections.

The next step in the procedure was to transform the detected position in the camera frame to a physical position on the Earth. To accomplish this, we first made the assumption that the ankles of the pedestrians in each video frame were located in a single plane at ground level. For each camera view, we annotated visually distinct locations in that plane which were visible both in the camera images and in georeferenced satellite orthoimagery. These locations included termini of dashed lane lines, street light poles, and corners of concrete structures. Using four corresponding locations, a perspective transformation matrix was used to map from screen space locations to latitude and longitude coordinates. This method assumed that the traffic camera was a rectilinear camera and that latitude and longitude represented a cartesian coordinate system. This was a reasonable assumption for the length (~100m) of the viewshed of each camera. Using this mapping for each pedestrian detected in each frame of camera video, the locations of the left and right ankles were transformed into latitude and longitude coordinates.

Finally, the detected pedestrians in each frame were tracked across frames. This was solved using the Munkres algorithm [9] implemented in the SciPy python library [10]. In this work, the Euclidean distance between detections in a transverse Mercator projection of the surface of the Earth was used. Other object tracking systems [11] use a distance metric computed using pixel locations in the camera image.

Pedestrian Analysis

The result of the video processing operation was a series of georeferenced time trajectories for each pedestrian visible. Pedestrians with left and right ankle detection confidence values below 40% were excluded. The position of each pedestrian was defined to be the mean position of their left and right ankles. Pedestrian velocities were determined using a Kalman filter to smooth out variations due to random sensor error and irregularities in the walk cycle. Pedestrian trajectories were then rotated into a coordinate system where the x axis was parallel to the centerline of the roadway and the y axis was perpendicular. The origin of the coordinate system was a point on the centerline of the road located on the edge of the crosswalk.

To analyze the mid-block crossing behavior of pedestrians, segments of each pedestrians' trajectory were selected where the velocity of the pedestrian was perpendicular to direction of vehicle travel and the position was within two standard lane widths (7.32m) of the centerline of the road. A maximum velocity deviation of 30 degrees from perpendicular was considered.

RESULTS

A total of 356 pedestrians were selected from March 29, 2020 to April 26, 2020. The dataset contained 333 mid-block and 23 crosswalk-adjacent pedestrians. Pedestrians who were more than one lane width (3.66m) from the crosswalk were considered to be crosswalk-adjacent. Figure 2 gives the trajectories of the pedestrians included in this study. The pedestrians visible in this study were primarily located around 10 meters away from the crosswalk due to the placement of the cameras. Figure 3 gives the speed distribution of crosswalk-adjacent and mid-block crossing pedestrians. The median pedestrian speed for mid-block crossings was 1.0 m/s, slower than the reference North American speed of 1.38 m/s used by Bosnia and Weidmann [1] and the crosswalk-adjacent speed in this dataset of 1.13 m/s. We hypothesize this may be due to the lack of pedestrian urgency created by the crossing sign. Future work will investigate the causation of this outcome.

DISCUSSION

This method of measuring pedestrian behavior has a number of limitations. First, the method assumes a perfect perspective mapping between the road surface, pedestrian feet locations, and the camera. Some image distortion was present as the traffic cameras were not ideal rectilinear cameras. Ideally, the projection of the center of mass of each pedestrian on the ground would be measured, but the centroid of the pedestrian's ankles was measured. Because the ankles are located above the ground, this caused the estimated pedestrian positions to be farther away from the camera than their true position. Because this error does not change significantly from frame to frame, it had a small effect on the velocity computed in this study.

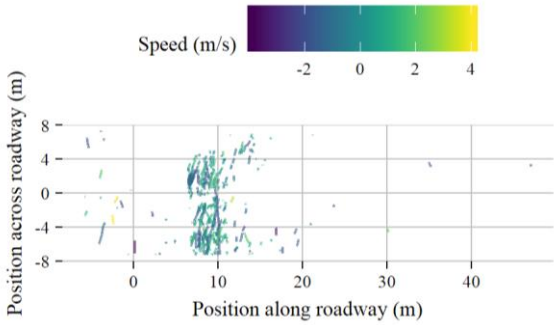

Figure 2. Pedestrian trajectory segments in Virginia traffic camera data where the pedestrian velocity was primarily perpendicular to the direction of vehicle travel.

This study methodology was not validated for detection accuracy. A future study will validate the detected pedestrian position against GNSS/GPS measurements. The pedestrian detection confidence threshold of 40% was chosen empirically. Future work will examine an ideal detection threshold.

CONCLUSION

The objective of this work was to develop a new method to study pedestrian behavior using traffic camera video. The method described in this work captures video of pedestrians from the Commonwealth of Virginia. Pedestrian trajectories were automatically detected from video. The median mid-block pedestrian crossing speed was 1.0 m/s, slower than values suggested by previous research. The median crosswalk-adjacent crossing speed was 1.13 m/s. We plan to investigate this further in future work.

NOVELTY/TRAFFIC SAFEY IMPLICATIONS

To the best of the knowledge of the authors, this work represents the first attempt to use pre-existing traffic camera video in the United States to characterize the behavior of vulnerable road users. This represents a new potential avenue for the understanding of all road users in crash, near-crash, and normal driving situations.

ACKNOWLEDGEMENTS

The authors acknowledge Advanced Research Computing at Virginia Tech for providing computational resources and technical support that have contributed to the results reported within this paper.

REFERENCES

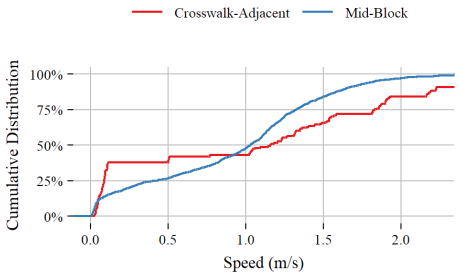

Figure 3. Distribution of pedestrian crossing speeds in Virginia traffic camera data.

[1] E. Bosina and U. Weidmann, "Estimating pedestrian speed using aggregated literature data," *Phys. Stat. Mech. Its Appl.*, vol. 468, pp. 1–29, Feb. 2017, doi: 10.1016/j.physa.2016.09.044.

[2] S. H. Haus, R. Sherony, and H. C. Gabler, "Estimated benefit of automated emergency braking systems for vehicle–pedestrian crashes in the United States," *Traffic Inj. Prev.*, vol. 20, no. sup1, pp. S171–S176, Jun. 2019, doi: 10.1080/15389588.2019.1602729.

[3] R. L. Knoblauch, M. T. Pietrucha, and M. Nitzburg, "Field Studies of Pedestrian Walking Speed and Start-Up Time:," *Transp. Res. Rec.*, Jan. 1996, doi: 10.1177/0361198196153800104.

[4] Virginia Department of Transportation, "Virginia 511 Web." https://www.511virginia.org/ (accessed Jul. 25, 2019).

[5] "Documentation." https://ffmpeg.org/documentation.html (accessed Apr. 14, 2020).

[6] S. Kreiss, L. Bertoni, and A. Alahi, "PifPaf: Composite Fields for Human Pose Estimation," in *The IEEE Conference on Computer Vision and Pattern Recognition (CVPR)*, Jun. 2019, [Online]. Available: https://github.com/vita-epfl/openpifpaf.

[7] "Huckleberry User Guide | Advanced Research Computing at Virginia Tech." https://arc.vt.edu/computing/huckleberry-user-guide/ (accessed Apr. 15, 2020).

[8] T.-Y. Lin *et al.*, "Microsoft COCO: Common Objects in Context," *ArXiv14050312 Cs*, May 2014, Accessed: Jul. 10, 2019. [Online]. Available: http://arxiv.org/abs/1405.0312.

[9] H. W. Kuhn, "The Hungarian method for the assignment problem," *Nav. Res. Logist. NRL*, vol. 52, no. 1, pp. 7–21, 2005, doi: 10.1002/nav.20053.

[10] P. Virtanen *et al.*, "SciPy 1.0: Fundamental Algorithms for Scientific Computing in Python," *Nat. Methods*, vol. 17, pp. 261–272, 2020, doi: https://doi.org/10.1038/s41592-019-0686-2.

[11] Z. Zhou, J. Xing, M. Zhang, and W. Hu, "Online Multi-Target Tracking with Tensor-Based High-Order Graph Matching," in *2018 24th International Conference on Pattern Recognition (ICPR)*, Aug. 2018, pp. 1809–1814, doi: 10.1109/ICPR.2018.8545450.

CHARACTERIZING DRIVER TAKEOVER ACCURACY: EFFECT OF AGE, SEX, STARTLE, AND SECONDARY TASK

Meta Austin
Center for Injury Research and Prevention, Children's Hospital of Philadelphia
Brown University School of Engineering

Madeline Griffith, Rahul Akkem, Jalaj Maheshwari, Thomas Seacrist, Kristy Arbogast, Valentina Graci
Center for Injury Research and Prevention, Children's Hospital of Philadelphia

INTRODUCTION

As autonomous vehicles become a reality, there will be instances in which drivers need to take over control of the vehicle to perform a crash-avoidance maneuver. Distractions will also be common since automation will allow engagement in secondary tasks [1]. Therefore, optimizing current driver-assist vehicle warnings is important across all populations of drivers. Young drivers in particular tend to dismiss forward collision warnings as false positive since they occur relatively early (1.7-2 s) before time of collision [2]. Female drivers tend to have a greater following distance in order to avoid nuisance alarms [2]. Specific to a takeover scenario in an autonomous driving situation, drivers may perform steering errors during these critical maneuvers and the accuracy of steering wheel control may differ across age and sex.

Autonomous vehicle technology may be designed to compensate for drivers overshooting or undershooting the correct steering wheel alignment. In our previous research, an Acoustic Startling Pre-Stimulus (ASPS) warning, which is defined as a 105 dB sound preceding a physical perturbation by 250 ms [3], was found to accelerate reaction times in male adult drivers during takeover actions in autonomous scenarios [4]. However, it is not clear if the ASPS also influences the accuracy of the takeover response.

The aims of this study are: to characterize takeover accuracy across age and sex and to examine the effect of the ASPS and a secondary task on steering wheel alignment in autonomous vehicle takeover scenarios.

METHODS

Fourteen adult (7 males) and 13 teenage (6 males) healthy driver volunteers participated in the study (Table 1). Participants' BMI was between the 5th and 95th percentile according to the subject's age and each held a valid driver's license. Adults were required to have had at least 5 years of driving experience and teenagers were required to have had at least 12 hours of driving experience in the last year. Participants were seated and belted on an oscillatory sled with their hands on their laps and instructed to align a marker on the steering wheel with a marker on a lateral post as fast as they could, as soon as the lateral sled perturbation started (peak acceleration 0.75 g). The angle between the two markers and the center of the wheel was 70° in the starting position. Two of the conditions included the ASPS occurring 250 ms before the sled motion at 105 dB for 40 ms [5]. Two of the conditions involved a secondary task that consisted of mobile texting while the sled started moving (see full method description [4]).

Table 1. Anthropometrics of study participants.

	N. of subjects	Age (years)	Height (cm)	Weight (kg)
Adult Males	7	25 – 37	177.9 ± 6.0	78.0 ± 12.9
Adult Females	7	25-28	168.6 ± 2.9	59.7 ± 3.5
Teenage Males	6	17	175.0 ± 7.0	68.4 ± 7.3
Teenage Females	7	16-17	168.3 ± 2.1	62.9 ± 5.6

Kinematics were collected with an 8-camera 3D motion capture system (NaturalPoint, IncOR). A custom-made Matlab (MathWorks, Inc., MA) program was used to extract the position of the steering wheel relative to the lateral post. The angle between these two markers was used to define the subject's steering wheel alignment angle in each trial as one of three possible outcomes: overshoot, undershoot, or correct alignment. Correct alignment was defined as aligning the steering wheel within 6° of exact alignment, where exact alignment is a 0°

difference between the steering wheel and lateral post positions [6]. Overshoot was defined as aligning the steering wheel more than 6° past exact alignment while undershoot was defined as aligning the steering wheel more than 6° short of exact alignment. The alignment angle and the proportion of trials with overshooting, undershooting, and correct alignment were calculated for each age group and across study conditions. The proportion of trials with overshooting, undershooting, and alignment were calculated as the percentage of the total number of trials for each group. Events like the manual takeover of an autonomous vehicle in a critical situation may not occur more than one time in a short period of driving. Therefore, we compared the first trial alignment angle with the alignment angle in the subsequent trials. We also assessed the influence of ASPS by age group and sex in the first trial only.

RESULTS

Correct alignment occurred in 20-29% of the trials depending on age, sex, and study group (Table 2). Adult female subjects reached correct alignment slightly more frequently than any other group. Adult females also overshot and undershot with equal frequency while all other groups overshot in around 50-60% of the trials. The proportion of correct alignment trials was not smaller with the secondary task (Table 2).

Table 2. Proportion of trials with overshooting, undershooting, and alignment across all trials for each group and set of conditions.

Group	Overshoot %	Undershoot %	Alignment %
Adult Males	61.8	18.18	20.0
Adult Females	35.7	35.7	28.6
Teen Males	52.1	25.0	22.9
Teen Females	64.3	14.3	21.4
ASPS	52.3	25.24	22.4
No ASPS	54.6	20.4	24.1
Sec. Task	44.9	29.97	25.2
No Sec. Task	62.0	16.7	21.3

The alignment angle decreased after the first trial for adult male subjects (Figure 1a). For adult female subjects the alignment angle only decreased after trial 3 and increased again in the last trial (Figure 1b). In contrast, for both male and female teens, the alignment angle showed no pattern and was variable across trials (Figures 1a,b).

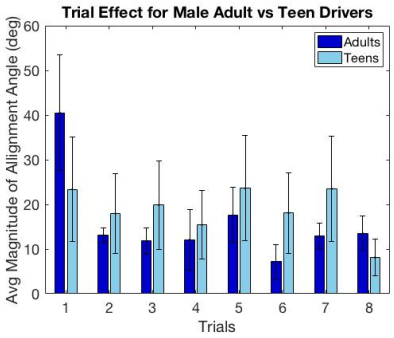

a.

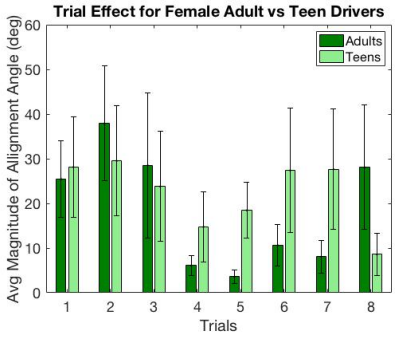

b.

Figures 1a,b Mean (SD) alignment angle for adult versus teen subjects for each sex across all trials.

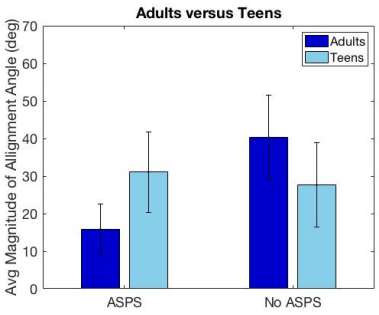

Figure 2. Mean (SD) magnitude of alignment angle in first trial for all adult versus all teen subjects, comparing trials with and without an ASPS.

Adult drivers had a reduced alignment angle when the first trial had an ASPS compared to when the first trial had no ASPS while teen drivers performed similarly with ASPS or without (Figure 2).

DISCUSSION

The aim of this study was to characterize takeover accuracy by age and sex in a simulated takeover scenario. A secondary aim was to understand the influence of the ASPS and a secondary task on takeover accuracy. The results showed that female adult drivers showed greater accuracy than any other age/sex group (28% vs 20-23%). Furthermore, when female adult drivers made steering errors, they were

equally as likely to overshoot as to undershoot in contrast to their male or younger counterparts who were more likely overshoot (Table 2).

Male adult drivers showed a rapid familiarization/learning effect: they decreased the alignment angle after the first trial (Figure 1a). Female adult drivers also showed a decrease of alignment angle, but only after the third trial and they increased the angle again in the last trial (Figure 1b). This suggests that female adult drivers might have taken longer to familiarize with the task, and after familiarization (in trials 4-7), they may experience fatigue or complacency (trial 8).

Teens did not show a familiarization/learning effect. Teens are known to have more risky driving behavior [7]. Previous research found that teens perform hard turns of the steering wheel more often than adults to avoid a crash [7] and they are more often involved in elevated g-force events [2, 7].

Adult drivers were more accurate in their takeover steering maneuver with the ASPS, suggesting that the ASPS warning system may be beneficial for adults. However, ASPS did not influence alignment angles in the teen driver groups. It is plausible that the 250 ms time between the ASPS and the start of the critical event (i.e. sled moving) may need to be different for teen drivers. Neuroscience studies shows that the teenage brain has a different physiology and development [7]. Therefore, the ASPS may be processed differently in teens.

The secondary task did not increase the alignment angle. However, previously, the same secondary task was found to increase takeover reaction times [1, 4]. Mobile texting may be more detrimental to the time taken to steer than to the accuracy of the steering action. The study presents some limitations. The study conditions were fully randomized, therefore the analysis on the first trial response with and without ASPS has few data points (11 with ASPS, 14 without ASPS). No instructions were given on how to reach for the steering wheel since we wanted to understand the natural behavior of the drivers during a critical autonomous scenario.

CONCLUSION

This study showed that takeover accuracy is influenced by sex, age, and a startle-based warning. Female adult drivers showed greater accuracy than any other age/sex groups. Overall, adult drivers show some alignment angle learning effect over time, while teen drivers' accuracy is variable over time. The ASPS improves accuracy of alignment but only in adult drivers. These findings may inform the design of future assistive steering technology that considers the diversity of the driving population.

NOVELTY/TRAFFIC SAFEY IMPLICATIONS

This is the first study characterizing the effect of age and sex on steering behavior in takeover scenarios. These findings can inform the design of future in-vehicle technology.

ACKNOWLEDGEMENTS

National Science Foundation (NSF) Center for Child Injury Prevention Studies at the Children's Hospital of Philadelphia (CHOP).

REFERENCES

1. Eriksson, A. & Stanton, N. A. Takeover Time in Highly Automated Vehicles: Noncritical Transitions to and From Manual Control. *Hum. Factors* **59**, 689–705 (2017).

2. Montgomery, J., Kusano, K. D., Hampton, &, Gabler, C. & Gabler, H. C. Age and Gender Differences in Time to Collision at Braking From the 100-Car Naturalistic Driving Study Age and Gender Differences in Time to Collision at Braking From the 100-Car Naturalistic Driving Study. *Traffic Inj. Prev.* **15**, (2014).

3. Mang, D. W. H., Siegmund, G. P., Inglis, J. T. & Blouin, J.-S. The startle response during whiplash: a protective or harmful response? *J. Appl. Physiol.* **113**, 532 LP – 540 (2012).

4. Graci, V. *et al.* The Effect of An Acoustic Startling Warning On Take-Over Reaction Time And Trunk Kinematics for Drivers in Autonomous Driving Scenarios. *63rd Stapp Car Crash Conference* 1–4 (2019).

5. Sutter, K., Nonnekes, J., Dibilio, V., Geurts, A. C. & Weerdesteyn, V. Does the StartReact effect apply to first-trial reactive movements? *PLoS One* **11**, 1–11 (2016).

6. Simons-Morton, B. G. *et al.* Crash and risky driving involvement among novice adolescent drivers and their parents. *Am. J. Public Health* (2011)

7. Simmonds, D. J., Hallquist, M. N. & Luna, B. Protracted development of executive and mnemonic brain systems underlying working memory in adolescence: A longitudinal fMRI study. *Neuroimage* **157**, 695–704 (2017).

Safety Benefit of Advanced Sensors in Pedestrian Automated Emergency Braking Systems

Samantha H. Haus, Hampton C. Gabler

Virginia Tech, Blacksburg, VA

INTRODUCTION

Automated emergency braking (AEB) has the potential to mitigate or avoid many vehicle-to-vehicle crashes, but AEB may not be as effective in preventing vehicle-to-pedestrian collisions. Pedestrians are more difficult for traditional AEB systems to detect than a vehicle because of their smaller size and different material properties. Current Pedestrian Automatic Emergency Braking (PAEB) systems use a combination of radar and cameras to detect an impending vehicle-pedestrian collision [1]. The combination of multiple sensor modalities increases the efficacy of pedestrian detection and reduces the likelihood of a false positive [2].

Advanced sensors, e.g. LIDAR, could improve PAEB performance. However, there is a tradeoff between the improved performance offered by advanced sensors and the associated cost for these higher capabilities. Radar and camera systems tend to have a narrow field of view (FOV) and may not detect all pedestrians in time to prevent the collision. LIDAR has a wider field of view and may substantially improve detection, but is more expensive. The objective of this study was to determine the influence of FOV and range on the effectiveness of PAEB systems to determine the potential benefit of advanced sensors.

METHODS

Data Source

This study utilized vehicle-pedestrian crashes from the Pedestrian Crash Data Study (PCDS). PCDS was collected from 1994-1998 and contains 549 vehicle-pedestrian crashes. PCDS inclusion criteria were frontal vehicle-pedestrian collisions involving late-model vehicles in which the vehicle was forward moving and the pedestrian was not lying down or sitting on the roadway. Each case contains detailed pedestrian injury information, reconstructed impact speeds, crash scene diagrams, and detailed vehicle damage reports which were used to simulate the crash.

AEB Model

The study developed a computational model for simulation of each PCDS cases with and without PAEB. The PAEB model was coded using the R programming language. The model was designed to iteratively step through time from before AEB system activation to impact. At each time step, the position, the velocity, and the acceleration of the vehicle and pedestrian were calculated.

The AEB system activated when four conditions were met: 1) the pedestrian was in the road, 2) the pedestrian was within the FOV and range of the sensor system (detectable), 3) the pedestrian was detectable for the length of latency period, and 4) the time-to-collision (TTC) threshold of activation was reached.

PCDS scene diagrams were manually analyzed to determine the distance from the point at which the pedestrian was in the road and visible until the impact point. If the crash scene diagram showed that the view of the pedestrian was obstructed, for example by a parked vehicle, then the pedestrian was defined to be “in the road” once they first became visible.

A variety of sensor FOV and ranges were considered for analysis. Commercially available LIDAR and radar systems specifications represented an ideal version of each sensor system. Pedestrian detection is difficult and the consequences of false positives could be detrimental to the occupant and to acceptance of the technology. Therefore, more realistic pedestrian ranges were examined for both LIDAR and radar. Li, et al. [3] concluded that LIDAR pedestrian detection was unsatisfactory at a range of 40-50 meters due to the sparse LIDAR point cloud. Belyaev, et al. [4] found that the maximum automotive range for pedestrian detection was 40-45 meters. The pedestrian was assumed to be detectable if they were in the road and within the angle and range of the sensor system. The sensor configurations examined in this study are shown in Table 1.

Table 1. Sensor configurations.

Configuration	Sensor Type	Sensor FOV	Sensor Angle
1	LIDAR	360°	250m
2	LIDAR	360°	50m
3	LIDAR	120°	50m
4	Radar	24°	160m
5	Radar	24°	40m

The latency period was defined as the sum of the time needed for the sensor to detect the pedestrian, the time needed for the system to recognize the pedestrian as a pedestrian, and the time needed for the vehicle to prime the brakes for the evasive braking maneuver. The latency threshold was varied from 0 – 0.4 seconds.

The time to collision (TTC) was calculated at each time step by dividing the distance to the impact point by the vehicle velocity. The system only activated once the TTC threshold was reached. The TTC threshold was varied from 0.5 – 2 seconds.

Once all four activation conditions were met, the AEB system activated. The AEB system was assumed to brake at a maximum of 0.8g (dry), 0.4g (wet), or 0.3g (icy) with a jerk of -30 m/s^3.

The iteration continued until the vehicle came to a stop or the vehicle and pedestrian missed each other. An impact was said to have occurred if at any time in the simulation the pedestrian came into contact with any part of the vehicle. The pedestrian was treated as a point mass, while the car size was assumed to be the track width and 1.2 times the wheel base length. It was assumed that the pedestrian took no avoidance actions.

AEB Model Inputs

The model required the vehicle and pedestrian's travel speed and trajectory in addition to the case environmental characteristics and vehicle parameters.

PCDS does not report travel speed for most cases, therefore we used the PCDS impact speed to estimate the vehicle travel speed. If PCDS reported no braking, the travel speed was set to the impact speed. If the driver reportedly braked, we assumed two different driver braking models: a late/hard and early/weak braking driver. The late/hard braking driver was assumed to brake at a TTC of 0.4 seconds and a max deceleration of 0.4 g, while the early/weak braking driver was assumed to brake at a TTC of 2 seconds and a deceleration of 0.2 g, regardless if the pedestrian was visible or not. The results shown in this study are the average of the driver braking models. More details on the travel speed estimation method can be found in Haus, et al. [5]. Pedestrian travel speeds were estimated based on the age of the pedestrian and whether or not they were in a group [6].

To calculate the trajectory points, we assumed the impact point was the origin. In a similar method to the calculation of the travel speed, we back calculated to estimate the distance at which the model driver braking started from the impact point. We assumed that the vehicle and the pedestrian traveled in a straight path perpendicular to each other. The longest TTC threshold we examined was two seconds. Therefore, we back calculated the trajectory points to a minimum of two seconds prior to impact to ensure the system had the full time to avoid the crash. We also assumed that the original impact point was located in the center of the vehicle. Therefore, if the vehicle braked enough that the pedestrian was able to walk further than half the width of the vehicle, then the crash was avoided because the vehicle missed the pedestrian even though the vehicle did not come to a complete stop.

RESULTS

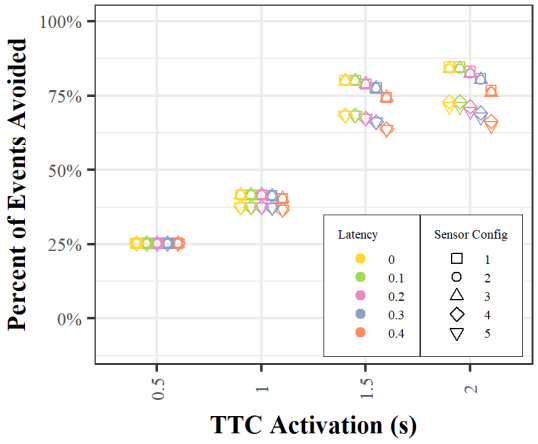

Figure 1. Percent of crashes avoided for a range of TTC and Latency values and across five sensor configurations.

As shown in Figure 1, when TTC threshold was increased and latency was decreased, the systems were able to avoid a larger percentage of the crashes. Systems with a larger FOV and a longer range were able to avoid a larger percentage of crashes. Although longer range sensor configurations performed better, sensor range had only a small effect on the overall crash avoidance. A 360° sensor system with a 250m range only avoided 0-1% more crashes than the same sensor system with a 50 meter range. Similarly, a 24° FOV sensor with a 160 meter range only avoided 0-2% more crashes than the same sensor system with a 40 meter range. An AEB system with a 0.5 second

TTC threshold was only able to avoid 25% of cases regardless of system latency and sensor configuration. Sensor configuration and latency had little effect on crashes avoided at TTC thresholds of one second and less. The most effective AEB system simulated avoided 85% of the pedestrian crashes.

DISCUSSION

While sensor configuration had an effect on the overall crashes avoided, the effect was smaller than expected. Range had at most a 2% difference in effectiveness while FOV had at most a 12% difference. This means that in many vehicle-pedestrian crashes, the pedestrian entered the road less than 40-50 meters from the vehicle and that most pedestrians were within a 24° FOV when they were detected. This is promising because it indicates that current technology ranges and FOV are sufficient to detect and potentially avoid most vehicle-pedestrian crashes, but we assumed all the cases were straight crossing cases. We expect sensor configuration will play a larger role in turning cases.

In this study we compared the maximum range of sensors on the market to the maximum ranges that were feasible for pedestrian detection. The ranges chosen for pedestrian detection may still be optimistic. It is possible that the sensors can only accurately detect pedestrians at lower ranges or may have shorter ranges during adverse weather conditions. In future work lower ranges should also be tested to evaluate how more conservative pedestrian detection system may affect the system ability to avoid crashes.

Additionally, this work only examined single sensor systems. Radar systems commonly have various FOVs and ranges within a system. For example they may have a long range radar with a FOV of ±6° and range of 160m coupled with a short range sensor with a FOV ±12° and range of 60 meter. Current systems often depend on both radar and cameras to detect pedestrians. While adverse weather may have only a small effect on radar and LIDAR, it has a large effect on camera detection. This was not accounted for in the model. Future work could combine multiple sensors and vary effectiveness based on weather conditions.

NOVELTY/IMPLICATIONS

This model is an improvement over previous AEB models using the PCDS data because the detection capability of the sensor system and pedestrian motion were considered [5]. This model utilizes estimated vehicle and pedestrian trajectories to evaluate spatial-temporal avoidance potential. The vehicle can avoid the pedestrian by coming to a complete stop prior to the impact point, i.e. spatial avoidance, or by slowing down enough that the pedestrian can cross without incident, i.e., temporal avoidance. The model utilizes simplified trajectories that assumed the vehicle and pedestrian were travelling perpendicular to one another. While in most crashes the pedestrian was traveling perpendicular to the vehicle, future work could improve the trajectories by including the true pedestrian and vehicle trajectories from the crash scene diagrams.

This study showed that pedestrian detecting AEB has the potential to avoid up to 85% of frontal vehicle-pedestrian collisions when only considering braking avoidance maneuvers. The addition of steering avoidance maneuvers could improve the avoidance potential. Systems with longer TTC thresholds and shorter latency values were able to avoid more crashes.

ACKNOWLEDGEMENTS

The authors would like to acknowledge the Toyota Collaborative Safety Research Center (CSRC) and Toyota Motor Corporation for funding this research study. We would also like to thank Rini Sherony of the Toyota CSRC for her insight.

REFERENCES

[1] R. Ono, W. Ike, and Y. Fukaya, "Pre-Collision System for Toyota Safety Sense," SAE Technical Paper 2016, Art. no. 2016-01-1458.

[2] T. Gandhi and M. M. Trivedi, "Pedestrian Protection Systems: Issues, Survey, and Challenges," *IEEE Transactions on Intelligent Transportation Systems*, vol. 8, no. 3, pp. 413-430, 2007.

[3] K. Li, X. Wang, Y. Xu, and J. Wang, "Density Enhancement-Based Long-Range Pedestrian Detection Using 3-D Range Data," *IEEE Transactions on Intelligent Transportation Systems*, vol. 17, no. 5, pp. 1368-1380, 2016.

[4] A. A. Belyaev, T. A. Suanov, I. O. Frolov, and D. O. Trots, "The Range of Pedestrian Detection with Automotive Radar," in *2019 Radiation and Scattering of Electromagnetic Waves (RSEMW)*, 2019, pp. 432-435.

[5] S. H. Haus, R. Sherony, and H. C. Gabler, "Estimated benefit of automated emergency braking systems for vehicle–pedestrian crashes in the United States," *Traffic Injury Prevention*, vol. 20, no. sup1, pp. S171-S176, 2019/06/12 2019.

[6] T. J. Gates, D. A. Noyce, A. R. Bill, and N. Van Ee, "Recommended Walking Speeds for Pedestrian Clearance Timing Based on Pedestrian Characteristics," *TRB Annual Meeting*, 2006, Art. no. 06-1826.

DEVELOPMENT OF AN OMNIDIRECTIONAL NECK FOR THE EVALUATION OF SPORTS AND AUTOMOTIVE PROTECTIVE EQUIPMENT

Graham Fonseca
The University of British Columbia

Peter Cripton and Sarah Romani
The University of British Columbia

INTRODUCTION

Safety devices meant to protect against SCIs and TBIs are often evaluated with the use of an anthropometric test device (ATD). No existing ATD closely represents the anatomy of a human neck despite the fact that the overall natural curvature of the cervical spine provides stability and the individual vertebral geometry defines the range of motion [1]. Currently, there is no single surrogate appropriate for the multiplane loading that often occurs in real-world scenarios [2]. Our long-term project objective is to create a biofidelic, omnidirectional, surrogate cervical spine that can represent three preparedness levels; asleep, awake and not braced, and awake and braced. This research, however, was a first step towards the overall objective, and aimed to produce a cervical, functional spinal unit (FSU) based on human anatomy. The goal was for the surrogate to exhibit "good" biofidelity according to ISO/TR 9790, a lateral impact response requirement to assess the biofidelity of a dummy (0≤ rating <2.6 is unacceptable, 2.6≤ rating <4.4 is marginal, 4.4≤ rating <6.5 is fair, 6.5≤ rating <8.6 is good and 8.6≤ rating ≤10 is excellent), with passive muscle properties simulating a sleeping individual, in quasi-static AR, LB, FE and CM.

METHODS

Requirements

1) Ensure surrogate disc kinematic results have an "excellent," level of biofidelity according to ISO/TR 9790.
2) Ensure surrogate ligament stiffness results are within 25 N/mm of linear cadaveric stiffness values.
3) Each sub-axial vertebra must have accurate anatomical geometry and will be constructed from a young healthy male's cervical CT scans.
4) The FSU should have a "good" level of biofidelity according to ISO/TR 9790, in comparison to quasi-static in-vitro tests, representing a sleeping individual.
5) Ensure FSU kinematic results have an "excellent," level of repeatability according to ISO/TR 9790.

Disc Design and Testing

A cervical CT scan containing a suitable C4-C5 FSU, the most commonly injured site [3], was used for the surrogate to be based on. 31-year-old Patient 5, with a height of 183 cm and mass of 80 kg, was selected as younger males are the most commonly injured [4], [5], [6]. Dr. Shun Yamamoto, a fellowship trained spine surgeon, helped determine the surface area and height of the disc based on the scans, and potential surrogate materials were cut accordingly. The Dynamight 8841 (Instron) was used for quasi-static compression testing of surrogate IVDs up to 800 N. The results were analyzed in Correlation and Analysis 3.6.1 (CORA, v3.6.1, Partnership for Dummy Technology and Biomechanics, Gamersheim, Germany) which is able to compare the curve of the surrogate material against the curve of a cadaveric specimen and provide a quantitative value for biofidelity according to ISO/TR 9790.

Ligament Design and Testing

Numerous materials were acquired in order to find surrogates that would be biofidelic in linear stiffness, when compared to cadaveric test results for the major cervical ligaments including the anterior longitudinal ligament (ALL), posterior longitudinal ligament (PLL), capsular ligament (CL), ligamentum flavum (LF) and interspinous ligament (ISL) [7]. Each surrogate was sheet-like and cut to 10 mm x 100 mm, except for the cylindrical Nanofiber (Nanofiber Solutions) which was provided with a 4 mm diameter. The Dynamight 8841 was used for tensile testing of ligaments, where they were each elongated to failure at quasi-static rates, and the linear stiffnesses were compared to published cadaveric values.

FSU-Bio Design and Testing

C4 and C5 were segmented from the CT scan slices of the subject, converted to 3D .stl files and imported into

SolidWorks (SW 64-bit, Student Engineering Kit 2017, Dassault Systems, France) where they were modified to include ligament attachment points for the five major cervical ligaments listed above. The vertebrae were 3D-printed in 316 SST and weighed. Dimensional accuracy was assessed by comparing CT scan slice dimensions to physical dimensions, as in Wu et al. [8] A sloped intervertebral disc was constructed next, in the same fashion as above, however, the posterior half of the middle layer was cut off and discarded, resulting in a posterior height of 3.18 mm. The ALL and CL were secured with set screws and the ISL was clamped with metal ferrules (Fig 1). Inclusion of the PLL and LF made FSU-Bio immovable, therefore they were not installed.

FSU-Bio was tested at quasi-static rates in the spine machine, which is able to apply a pure AR, LB or FE torque to the centre of a spine segment. The kinematic results were captured with an optoelectronic motion analysis system, Optotrak (Northern Digital Inc.) and torque load cell TRT-200 (Transducer Techniques).

CORA was used to assess biofidelity, in which published cadaveric displacement (°) vs. torque (Nm) results from any FSU between C3 and C7 were used as a reference. This is because C3-C7 are thought to be similar [9]. The tests were repeated, and analyzed in CORA, in order to asses repeatability. The construction process was assessed using CORA by deconstructing FSU-Bio, replacing the soft tissues and reconstructing the surrogate.

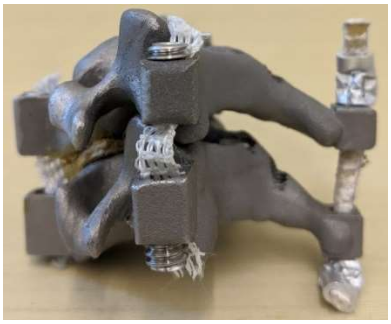

Figure 1. FSU-Bio

RESULTS

IVD fibre material CS301 (Moen) was the most biofidelic material, achieving an "excellent" score when compared to cadaveric test results from Cripton [10]. Poly-tape (Neoligaments) was suitable for the ALL and CL, and Nanofiber was suitable for the ISL, as they all fell within 25 N/mm of cadaveric values from Mattucci [7]. The vertebrae have a maximum dimensional error of 3.03 mm, the mass of C4 was 127 g and the mass of C5 was 124 g, 3.5 and 3.3 times more than cadaveric values, respectively [11].

FSU-Bio produced a "good" level of biofidelity in flexibility tests. When FSU-Bio was deconstructed, and constructed again with unused soft tissues, the biofidelity remained "good." FSU-Bio was deemed repeatable as it achieved an "excellent" score in all main and coupled motions when repeatedly tested.

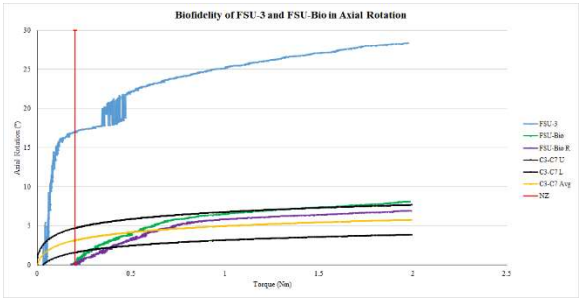

Figure 2. FSU-Bio

DISCUSSION

The effect of the vertebral mass on the inertia of the neck, and ultimately the head, during high speed and/or impact testing of FSU-Bio is unknown. The surrogate soft tissue's viscoelastic properties have not been characterized, resulting in the same issue. High speed and/or impact tests should be carried out to determine the biofidelity in these situations.

The dimensional errors were less than 1.25 mm, small enough to suggest user error in measurement, with the exception of vertebral body width for both C4 and C5. Ideally, the ground truth would be made from a cadaveric specimen. For this reason, along with the low error for all other dimensions, it is reasonable to believe that the ground truth was measured incorrectly. Moving forward, 3D-printing in 316 SST is a viable production method.

A major strength of this research was the use of a patient's cervical CT scans as the anatomical basis for vertebral and disc geometry. Current ATD necks use rough approximations of human anatomy which makes it difficult to match human kinematics as individual vertebral geometry defines the ROM of the neck [1] and the height of the disc impacts the ROM [12]. Additionally, using a patient specific model means that the surrogate is based on an existing human, making the results more relevant to real-life applications.

Focusing on the intervertebral kinematics and soft tissues of a surrogate neck during the design phase is novel and is believed to influence biofidelity, as the neck controls the motion of the head. Ideally, kinetic and kinematic results from Patient 5 would be used for biofidelic analyses, however, the bottom-up approach using cadaveric comparisons is thought to produce better results than the typical top-down approach.

FSU-Bio is an osteoligamentous surrogate which is a limitation as musculature has an impact on the stability and strength of the spine [13], [14], which would alter

the kinetics and kinematics. Musculature that replicates the entire force-displacement and force-velocity curves of cadaveric musculature [15] should be included to increase biofidelity.

CONCLUSION

FSU-Bio showed good biofidelity in all main and coupled motions and ultimately achieved the goal that this research set out to accomplish. The use of ligaments in anatomically correct locations, discs and vertebrae based on the anatomy of a living person, and disc and ligament selection based on kinematic test results are all novel to the author's knowledge. FSU-Bio provides a foundation for the development of a surrogate C3-C7 segment, and help achieve the final goal of a biofidelic surrogate neck.

NOVELTY/TRAFFIC SAFEY IMPLICATIONS

Once this final model is created, standards, such as the Federal Motor Vehicle Safety Standard (FMVSS) will yield more meaningful results. For example the FMVSS 208, a standard regulating safety in the USA, uses head injury criteria (HIC) and neck injury criteria (N_{ij}) to assess safety equipment in cars. If the surrogate neck is more biofidelic than current surrogates, the HIC and Nij calculations will yield more accurate results, better informing the performance of safety equipment.

ACKNOWLEDGEMENTS

I would like to thank Dr. Brian Kwon, Leilani Reichl and Dr. Shun Yamammoto for their support in CT scan retrieval as well as ICORD and OIBG for the use of their facilities. I would also like to thank the National Sciences and Engineering Research Council for funding.

REFERENCES

[1] I. A. Kapandji, *The Physiology of the Joints: Volume Three: The Trunk and the Vertebral Column*, 2nd ed., vol. 3. London, UK: Churchill Livingstone, 1974.

[2] T. S. Nelson and P. A. Cripton, "A new biofidelic sagittal plane surrogate neck for head-first impacts," *Traffic Inj. Prev.*, vol. 11, no. 3, pp. 309–319, Jun. 2010, doi: 10.1080/15389581003614870.

[3] V. Prasad, A. Schwartz, R. Bhutani, P. Sharkey, and M. Schwartz, "Characteristics of injuries to the cervical spine and spinal cord in polytrauma patient population: experience from a regional trauma unit," *Spinal Cord*, vol. 37, no. 8, pp. 560–568, Aug. 1999, doi: 10.1038/sj.sc.3100878.

[4] A. Singh, L. Tetreault, S. Kalsi-Ryan, A. Nouri, and M. Fehlings, "Global prevalence and incidence of traumatic spinal cord injury," *Clin. Epidemiol.*, vol. 6, pp. 309–331, Sep. 2014, doi: 10.2147/CLEP.S68889.

[5] R. Nguyen *et al.*, "The International Incidence of Traumatic Brain Injury: A Systematic Review and Meta-Analysis," *Can. J. Neurol. Sci. J. Can. Sci. Neurol.*, pp. 1–12, Sep. 2016, doi: 10.1017/cjn.2016.290.

[6] "Rates of TBI-related Emergency Department Visits by Age Group — United States, 2001–2010.," *Centers for Disease Control and Prevention*, Jan. 22, 2016. https://www.cdc.gov/traumaticbraininjury/data/rates_ed_byage.html (accessed Dec. 07, 2019).

[7] S. F. E. Mattucci, "Strain rate dependent properties of younger human cervical spine ligaments," University of Waterloo, Waterloo, ON, 2011.

[8] A.-M. Wu *et al.*, "The Accuracy of a Method for Printing Three-Dimensional Spinal Models," *PLOS ONE*, vol. 10, no. 4, p. e0124291, Apr. 2015, doi: 10.1371/journal.pone.0124291.

[9] R. Drake, W. Vogl, and A. Mitchell, *Gray's Anatomy*, 1st ed. Philadelphia, PA, USA: Churchill Livingstone, 2012.

[10] P. A. Cripton, "Load Sharing in the Human Cervical Spine," Queen's University, Kingston, 1999.

[11] D. L. A. Camacho, R. W. Nightingale, J. J. Robinette, S. J. Vanguri, D. J. Coates, and B. S. Myers, "Experimental flexibility measurements for the developement of a computational head-neck model validated for near-vertex head impact," Lake Buena Vista, Florida, 1997, pp. 473–486.

[12] W. Yuan, H. Zhang, X. Zhou, W. Wu, and Y. Zhu, "The Influence of Artificial Cervical Disc Prosthesis Height on the Cervical Biomechanics A Finite Element Study.pdf," *World Neurosurg.*, vol. 113, pp. e490–e498, May 2018, doi: 10.1016/j.wneu.2018.02.062.

[13] M. M. Panjabi, A. A. White, and R. M. Johnson, "Cervical spine mechanics as a function of transection of components," *J. Biomech.*, vol. 8, no. 327, p. 336, 1975.

[14] M. M. Panjabi, T. Miura, P. A. Cripton, J. L. Wang, A. S. Nain, and C. DuBois, "Development of a system for in vitro neck muscle force replication in whole cervical spine experiments," *Spine*, vol. 26, no. 20, pp. 2214–9, Oct. 2001.

[15] G. P. Siegmund, D. D. Chimich, and B. S. Elkin, "Role of Muscles in Accidental Injury," in *Accidental Injury*, The Medical College of Wisconsin Inc on behalf of Narayan Yoganandan, N. Yoganandan, A. M. Nahum, and J. W. Melvin, Eds. New York, NY: Springer New York, 2015, pp. 611–642.